Intersubband cavity polaritons: The role of higher photonic modes

M. Załużny and W. Zietkowski
Institute of Physics, Maria Curie-Skłodowska University, Pl. M. Curie-Skłodowskiej 1, 20-031 Lublin, Poland
(Received 23 June 2009; revised manuscript received 13 October 2009; published 1 December 2009)

We present a theoretical analysis of the consequence of coupling between higher photonic modes and intersubband excitations in microcavities with embedded multiple quantum wells (MQWs). The polariton dispersion relations and angle-resolved absorption spectra are calculated numerically using a semiclassical approach based on a transfer-matrix formulation and effective-medium approximation. The obtained results are interpreted employing a multiple coupled harmonic-oscillator model supplemented by the input-output formalism. We show that when the MQW occupies a large fraction of space between cavity mirrors the coupling with higher photonic modes cannot be considered as a negligibly small perturbation in formation of the intersubband cavity polariton modes. When appropriate conditions are fulfilled the coupling between higher photonic modes and so-called "dark" intersubband electronic excitations can lead, in accordance with experimental results, to the formation of complex multiple-peaked absorption spectra.

DOI: 10.1103/PhysRevB.80.245301 PACS number(s): 78.67.Pt, 42.50.Hz

I. INTRODUCTION

Semiconductor microcavities (MCs) with embedded multiple quantum wells (MQWs) represent a convenient system to study fundamental light-matter interactions modified by the presence of a cavity as well as by two-dimensional (2D) electron confinement. A ground Fabry-Perot mode of the MC can be brought into resonance (by varying the external angle of incidence φ) with intersubband transitions in QWs. If their interaction energy is greater than any homogeneous (or inhomogeneous) broadening of bare photon or intersubband mode, the system is in the strong-coupling regime (SCR), first observed in 2003 (Refs. 1 and 2) (in agreement with earlier semiclassical predictions[3,4]). In this regime, the eigenstates of the system are the mixed states of light and matter, called polaritons. Their energy eigenvalues are modified substantially with respect to those in the absence of the coupling. The normal-mode splitting breaks the degeneracy of the ground photonic mode and intersubband transitions into lower (L_1) and upper (U_1) polariton branches. Their behavior is well described by a simple model of two-coupled harmonic oscillators. The minimal splitting between the upper and lower branches is referred to in literature as Rabi splitting $2\Omega_{R_{res}}(\equiv 2\Omega^{(1)}_{R_{res}})$. The above-mentioned polaritons appear in linear optics as quasinormal modes of the systems and manifest themselves as two optical resonances (peaks) in the angle-resolved absorption spectra.[3–6] The angular dependence of these peaks (modes) can be also modeled by the two-oscillator model. However, the minimal separation between the modes $2\bar{\Omega}_{R_{res}}(\equiv 2\bar{\Omega}^{(1)}_{R_{res}})$ is larger than the Rabi splitting $2\Omega_{R_{res}}$.[5,6] It is the consequence of the fact that even at the resonance the above-mentioned dips are connected with polariton modes having different in-plane wave vectors.

Since the initial work, many important developments have followed. These include the electrical control of the Rabi splitting[7,8] and the realization of electroluminescent devices based on intersubband cavity polaritons.[9–11] The above-mentioned achievements open the way to the development of inversionless mid and far-infrared lasers, with lower threshold with respect to quantum cascade lasers. Moreover, recently published theoretical and experimental results[12] also indicate that in the case of nonadiabatic switching of the ultrastrong light-matter coupling in semiconductor MCs ($2\Omega_{R_{res}}$ comparable with the intersubband frequency ω_{IT}) new exciting quantum electrodynamical phenomena should occur. The giant mode splitting ($2\bar{\Omega}_{R_{res}}$ comparable with ω_{IT}) has already been observed in the mid-infrared region ($\lambda \sim 10\ \mu$m) (Refs. 5, 13, and 14) and the THz region ($\lambda \sim 100\ \mu$m).[15]

In the above-mentioned new developments MCs containing a large number of the QWs are usually used. It is connected with the fact that the use of a large number of QWs helps to achieve a large value of $2\Omega_{R_{res}}$. Thus, the full understanding of the strong coupling between MCs modes and intersubband transitions, in the case when optically active material, i.e., MQW extends nearly over the whole length between mirrors (bulk MCs), is an important issue. Experimental results recently published by Dupont *et al.*[2,14] indicate that the above-mentioned problem is far from complete understanding. The authors observed, contrary to the prediction based on a single mode cavity approximation commonly used in the literature, the formation of the additional strong absorption peak between the U_1 and L_1 polariton branches, on the low-energy side of the intersubband resonance. At this point it is also appropriate to note that numerical simulations based on the transfer-matrix formalism (TMF) predict the formation of a small central peak even in the case of more complex systems, namely, the quantum cascade light emitters working in the SCR.[9,16]

The results reported by Dupont *et al.*[2,14] are interpreted using a simplified approach based on semiclassical linear dispersion theory.[17] Unfortunately, such an approach does not allow for detailed clarification of the nature of the polariton modes responsible for the additional central peak. It is obvious that in order to get valuable information on the nature of the additional polariton modes supported by the bulk microcavities (BMCs) we must go beyond the above-mentioned single mode cavity approximation. Unfortunately, the literature on the coupling between higher photonic modes and the electronic excitations in semiconductor MCs is

scarce and limited to the excitonic polaritons in the Bragg mirror based MCs. In Ref. 18 (Ref. 19) the authors discussed the formation of the additional polaritonic modes due to the coupling between excitons and higher cavity modes (Bragg modes). Some papers have also been published investigating the polariton modes formed by pairwise interaction between exciton and (lateral) photon modes of like spatial symmetry in semiconductor MCs with 2D optical confinement.[20] In a recently published paper Kondo *et al.*[21] report the observation of multiple peaks in the transmission spectra of single-crystalline organic MC. The dispersion relations for the cavity polaritons are obtained at normal incidence as a function of thickness of the MC. The form of these relations indicates the participation of higher photonic modes in formation of the polariton modes responsible for the above-mentioned multiple-peaked spectra.

In this paper we employ two approaches to the problem of the influence of higher photonic modes on the properties of the intersubband polaritons supported by the $\lambda/2$ and $\lambda/4$ BMCs with totally reflecting back mirror. (Some preliminary results concerning the $\lambda/2$ BMCs have already been published.[6]) We present a semiclassical analysis based on the TMF and the effective-medium approximation (EMA).[22] It shows that the multiple peak features appearing in the angle-resolved absorption spectra of the above-mentioned systems can be successfully described employing the concept of the constant angle intersubband radiative polaritons. To get a better insight into the nature of the intersubband cavity polaritons supported by the BMCs we also present the discussion based on the framework of multiple coupled harmonic-oscillator model[18,23–26] (MCHOM) supplemented by input-output formalism.[27] The advantage of this approach is that employing the concept of the "bright" and "dark" intersubband states[18,24,28] we can obtain simple analytical solutions even when higher photonic modes are taken into account. Consequently, the dependency of the position, width, and height of peaks on different parameters can be easily visualized and predicted.

The rest of this paper is organized as follows. Section II provides the theoretical framework. The description of the considered systems and the uncoupled modes supported by them are outlined in Sec. III. Numerical results are presented and discussed in Sec. IV. Section V contains concluding remarks.

II. THEORETICAL FRAMEWORK

A. Semiclassical approach

To keep the discussion as self-contained as possible, in this subsection (and Appendix A) we summarize the essential ingredients of the TMF (and the EMA) that we shall need for our purpose.

1. Transfer-matrix formalism

Let us consider a typical stratified structure that consists of a stack of $1,\ldots,j,\ldots,m$ plane-parallel layers (with thickness d_j and dielectric constant ε_j) sandwiched between two semi-infinite substrate (0) and cladding $(m+1)$ media. For convenience we assume that all the above-mentioned media are isotropic and homogeneous. The MQW (with N_{QW} symmetric and equidistant QWs) is located between the media j and $j+1$. Each period of the MQW consists of the QW (with thickness L_{QW}) sandwiched between half barrier layers with thickness $\bar{d}_b = d_b/2 = (L_{\mathrm{MQW}} - L_{\mathrm{QW}})/2$, where L_{MQW} denotes the period of the MQW structure. In numerical simulations we take into account the difference between the dielectric constant of the well (ε_w) and barrier (ε_b) materials.

The monochromatic light (polarized in the x-z plane) incidents from the substrate medium $(\varepsilon_s \equiv \varepsilon_0)$ at the angle $\varphi \equiv \varphi_0$ with respect to the growth direction z. The repeated application of the Snell's law gives

$$\varepsilon_0^{1/2} \sin \varphi_0 = \cdots = \varepsilon_j^{1/2} \sin \varphi_j = \cdots = \varepsilon_{m+1}^{1/2} \sin \varphi_{m+1}, \quad (1)$$

where φ_j is the angle of refraction of the jth medium. In the considered geometry there is only a single component of the magnetic field $\mathbf{H}(\mathbf{r},t) = \mathbf{e}_y H_y(z) e^{\mathrm{i}(k_x x - \omega t)}$ in each medium. $k_x = \varepsilon_s^{1/2} \omega \sin \varphi / c$ is the in-plane component of wave vector. The relation between amplitudes of the magnetic field in the q and $p(>q+1)$ media may be generally written in the following form:[22]

$$\begin{bmatrix} H_{l+}^{(q)} \\ H_{l-}^{(q)} \end{bmatrix} = \mathbf{T}_{q,p} \begin{bmatrix} H_{u+}^{(p)} \\ H_{u-}^{(p)} \end{bmatrix}, \quad (2)$$

where $H_{\alpha+}^{(n)}$ and $H_{\alpha-}^{(n)}$ $(\alpha = l,u)$ are the complex amplitudes of the magnetic field corresponding to the waves traveling in positive and negative z directions, respectively. The subscript l (u) indicates that we take the amplitude with respect to the plane $z_{n-1,n}$ $(z_{n,n+1})$ separating the media $n-1$ and n (n and $n+1$). At this point it is worth noting that the TMF is commonly used for modeling wave propagation in stratified media based on MQWs (see, e.g., Ref. 29). However, they can take different forms depending on where the field amplitudes or the field components form the basis set. In our approach the TMF is based on the amplitudes of the upward and downward propagating waves.

The total 2×2 transfer matrix of the system $\mathbf{T} \equiv \mathbf{T}_{0,m+1}$ can be considered as a product of matrices that describe the effects of individual interfaces and layers of the entire structure as well the MQW (Refs. 22 and 29)

$$\mathbf{T} = \mathbf{I}_{0,1}\mathbf{L}_1\mathbf{I}_{1,2}\cdots\mathbf{I}_{j,b}\mathbf{T}^{\mathrm{MQW}}\mathbf{I}_{b,j+1}\cdots\mathbf{I}_{m-1,m}\mathbf{L}_m\mathbf{I}_{m,m+1}. \quad (3)$$

The matrix $\mathbf{L}_j$ describes the effect of propagation through the jth layer. In the case of the homogeneous (isotropic or uniaxial) layer it has the form

$$\mathbf{L}_j \equiv \mathbf{L}(\beta_j) = \begin{bmatrix} \exp -i\beta_j & 0 \\ 0 & \exp i\beta_j \end{bmatrix}, \quad (4)$$

where $\beta_j = k_z^{(j)} d_j$ and $k_z^{(j)}$ is the normal component of the wave vector in jth material. When this material is isotropic $k_z^{(j)} = \sqrt{\varepsilon_j K^2 - k_x^2}$ and $(K = \omega/c)$.

The matrix $\mathbf{I}_{i,j}$, accounting for the interface between the homogeneous media (layers) i and $j(=i+1)$, is given by

$$\mathbf{I}_{i,j} = \mathbf{I}_{j,i}^{-1} = \mathbf{I}(r_{i,j}) \equiv \frac{1}{t_{i,j}} \begin{bmatrix} 1 & r_{i,j} \\ r_{i,j} & 1 \end{bmatrix}, \tag{5}$$

where $r_{i,j}(t_{i,j})$ is the Fresnel reflection (transmission) coefficient for the interface i-j [see Eqs. (8) and (9)].

The transfer matrix through the MQW can be written in the form

$$\mathbf{T}^{\mathrm{MQW}} = [\mathbf{L}(\beta_b/2)\mathbf{I}(r_{b,w})\mathbf{L}^{\mathrm{QW}}\mathbf{I}(r_{w,b})\mathbf{L}(\beta_b/2)]^{N_{\mathrm{QW}}}, \tag{6}$$

where $\mathbf{L}(\beta_b/2)$ is the transfer matrix through the halves of the barriers surrounding the QW. $\mathbf{L}^{\mathrm{QW}}$ is the transfer matrix through the well layer [containing a quasi-two-dimensional electron gas (Q2DEG)] located between semi-infinite media with the dielectric constant ε_w. Like in the previous papers[4,22,30,31] we assume for simplicity that light induced current density $\mathbf{j}$ in each QW can be regarded as being localized only in the well layer. In general, the QW region should be described by a nonlocal (anisotropic) susceptibility evaluated by linear-response theory. Fortunately, the problem simplifies greatly when the wavelength of the radiation is much smaller than L_{MQW}. When the above condition is fulfilled the EMA can be employed. In this approximation the MQW is modeled by an effective uniform uniaxial medium with the diagonal dielectric tensor $\varepsilon_{\alpha\beta}=\delta_{\alpha\beta}\varepsilon_{\alpha\alpha}$ (for details see Appendix A).

The total transfer matrix [Eq. (3)] reduces now to the form

$$\mathbf{T} = \mathbf{I}(r_{0,1}) \cdots \mathbf{I}(r_{j,j'})\mathbf{L}(\beta_{j'})\mathbf{I}(r_{j',j+1}) \cdots \mathbf{I}(r_{m,m+1}), \tag{7}$$

where $\beta_{j'} \equiv \beta_{\mathrm{MQW}} = k_z^{(j')} d_{j'}$, $d_{j'} \equiv d_{\mathrm{MQW}} = N_{\mathrm{QW}} L_{\mathrm{MQW}}$ is the thickness of the MQW and

$$k_z^{(j')} \equiv k_z^{(\mathrm{MQW})} = [\varepsilon_{xx}K^2 - (\varepsilon_{xx}/\varepsilon_{zz})k_x^2]^{1/2}.$$

The Fresnel reflection and transmission coefficients for the interface κ-υ can be written as

$$r_{\kappa,\upsilon} = (k_z^{(\kappa)}\bar{\varepsilon}_\upsilon - k_z^{(\upsilon)}\bar{\varepsilon}_\kappa)/(k_z^{(\kappa)}\bar{\varepsilon}_\upsilon + k_z^{(\upsilon)}\bar{\varepsilon}_\kappa), \tag{8}$$

$$t_{\kappa,\upsilon} = 2k_z^{(\kappa)}\bar{\varepsilon}_\upsilon/(k_z^{(\kappa)}\bar{\varepsilon}_\upsilon + k_z^{(\upsilon)}\bar{\varepsilon}_\kappa), \tag{9}$$

where $\bar{\varepsilon}_\upsilon = \varepsilon_\upsilon$ for $\upsilon \neq j'$ and $\bar{\varepsilon}_\upsilon = \varepsilon_{xx}$ for $\upsilon = j'$.

2. Basic equations

The overall amplitude reflection coefficient of the structure (r) is connected with the total transfer-matrix $\mathbf{T}$ components by relation

$$r = T_{21}/T_{11}. \tag{10}$$

As it was mentioned, in this paper we discuss the MCs with totally reflecting back mirror. In other words, we work in the regime of total internal reflection (TIR).[22] It implies the following expression for the absorptance of the structure:

$$A = 1 - |r|^2. \tag{11}$$

The dispersion relations for the electromagnetic modes supported by the structure can be derived from the requirement

$$T_{11} = 0 \tag{12}$$

equivalent to the condition that in the semi-infinite media 0 and $(m+1)$ incoming waves do not exist, i.e., $H_{l+}^{(0)} = H_{u-}^{(m+1)} = 0$. Note that the solutions of Eq. (12) correspond to the poles of the reflectivity r. The above-mentioned solutions can be divided into radiative and nonradiative modes.[32] We will concentrate on the radiative modes since only these modes are accessible by angle-resolved reflectance-absorptance measurement. The frequencies of the radiative modes are complex even in the dissipationless limit. We are interested in the (constant angle) modes radiating energy into the substrate medium at a fixed and real angle φ. One can show that in the case of the ιth constant angle radiative mode not only the eigenfrequency ($\tilde{\omega}_\iota = \omega_\iota + i\omega_\iota''$) but also the wave vector ($\tilde{k}_{x,\iota} = k_{x,\iota}' + ik_{x,\iota}''$) should be treated as complex quantities satisfying the relation $\tilde{k}_{x,\iota}/\tilde{\omega}_\iota = |\tilde{k}_{x,\iota}/\tilde{\omega}_\iota|$.[32] Equivalently, we may also write that

$$\sin\varphi = \left(\frac{\tilde{k}_{x,\iota}}{\tilde{\omega}_\iota}\frac{\varepsilon_s^{1/2}}{c}\right) = \left(\left|\frac{\tilde{k}_{x,\iota}}{\tilde{\omega}_\iota}\right|\frac{\varepsilon_s^{1/2}}{c}\right). \tag{13}$$

The νth mode can be treated as a well-defined entity only when $|\omega_\iota''/\omega_\iota'| \ll 1$. Let us assume that this mode is spectrally separated from the rest of the modes. Then, for ω close to ω_ν' the absorptance of the structure is determined mainly by the resonant contribution from the above-mentioned mode (a single-pole approximation). Making appropriate expansions one finds that this contribution takes the following Lorentzian form (see Appendix B):

$$A_\nu(\omega) = \mathcal{A}_\nu \frac{1}{1 + (\omega - \omega_\nu')^2/\gamma_\nu^2} \tag{14}$$

with

$$\mathcal{A}_\nu = 4\gamma_\nu^{rad}\gamma_\nu^{abs}/\gamma_\nu^2, \tag{15}$$

where $\tilde{\omega}_\nu = \omega_\nu' + i\omega_\nu''$ ($\tilde{\omega}_\nu = \omega_\nu' + i\omega_\nu''$) denotes the νth mode frequency obtained including (neglecting) absorption in all components of the structure, $\gamma_\nu \equiv -\omega_\nu''$ and $\gamma_\nu^{rad} \equiv -\omega_\nu''$. In other words, the quantity γ_ν (γ_ν^{rad}) determines the total (radiative) polariton mode damping rate. For convenience we have also defined the absorptive decay rate $\gamma_\nu^{abs} = \gamma_\nu - \gamma_\nu^{rad}$ of the νth mode.

From Eq. (14) we find that a well-separated mode ν can be associated with a Lorentzian shape maximum in the angle-resolved absorptance of width $2\gamma_\nu$ centered at ω_ν'. The height of the peak reaches the maximum ($\mathcal{A}_\nu = 1$) when $\gamma_\nu^{rad} = \gamma_\nu^{abs}$. It is worth noting that we derived the above equation without referring to a concrete structure. Thus this equation is valid for an arbitrary MQW-MC structure provided that we work in the TIR configuration.

B. Multiple coupled harmonic-oscillator model

The MCHOM is commonly used in the literature for the description of cavity polaritons resulting from the coupling between ground cavity mode and excitons in QWs.[18,23–26] It has a good justification when the power transmission coeffi-

cients of the mirrors are very small. In this section we show that the above model is also useful for the study of intersubband cavity polaritons even when we go beyond a single cavity mode approximation. We assume for simplicity that the penetration of light into the mirrors is negligibly small. More precisely, we assume that the z component of the electric field associated with nth cavity mode $[E_z^{(n)}(z)]$ has nodes at the surfaces of the (dielectric) mirrors i.e., at $z=0$ and $z=L_{\mathrm{MC}}$ (see Appendix D). (Extension on the case when back mirror is metallic is straightforward.) We also omit differences between the dielectric constant of the barrier (ε_b), the well (ε_w), and the substrate (ε_s) materials.

1. Coupling between electronic and photonic modes

Initially, for the purpose of calculating the MC polariton dispersion, the coupling mirror is assumed to be perfect and no dissipation mechanism is included.[18] According to a standard MCHOM the intersubband electronic modes supported by different QWs are treated as independent oscillators having the frequency ω_{IT}. This frequency is assumed to be independent on the in-plane component of the wave vector q_x. The photonic modes c_n $(n=1,2,3,\ldots)$ are also treated as harmonic oscillators. The frequency of the nth photonic oscillator with the in-plane wave vector k_x is given by $\omega_{c_n}^2(k_x)=k_x^2c^2/\varepsilon_w+n^2\omega_\perp^2$, where $\omega_\perp^2=k_{z,1}^2c^2/\varepsilon_w$ and $k_{z,n}=n\pi/L_{\mathrm{MC}}$. For convenience in this paper we use a notation in which the photonic mode index coincides with the number of the antinodes of the mode.

The electronic oscillator (located at $z=z_\kappa$ with $\kappa=1,2,3,\ldots,N_{\mathrm{QW}}$) couples to the nth photonic mode, having the in-plane wave vector $k_x=q_x$, with the strength

$$V_{n\kappa}(k_x)=V_{\max}\sin\theta_n\mathcal{E}_n(z_\kappa), \tag{16}$$

where $\theta_n\equiv\theta_n(k_x)=\arcsin(k_x/\sqrt{k_x^2+k_{z,n}^2})$ and $\mathcal{E}_n(z)=\sin(zn\pi/L_{\mathrm{MC}})$ is the cavity mode function describing the spatial variation in $E_z^{(n)}(z)$. The product $V_{\max}\sin\theta_n$ denotes the coupling strength between c_n mode (the photonic oscillator) and the electronic oscillator situated at the antinode of the $E_z^{(n)}(z)$ field ($|\mathcal{E}_n|=1$). The geometrical factor $\sin\theta_n$ originates due to the well-known polarization selection rules of the intersubband transitions. The coupling parameter $V_{\max}$ can be taken in the following form:[11]

$$V_{\max}\cong\sqrt{2\pi e^2\mathcal{N}_s/m^*\varepsilon_wL_{\mathrm{MC}}}, \tag{17}$$

where $\mathcal{N}_s=N_s^{(1)}f_{12}$ is the product of the surface electron concentration in the ground subband $|1\rangle$ and the oscillator strength corresponding transition from the ground $|1\rangle$ to excited subband $|2\rangle$ (see Appendix A). [The result consistent with Eq. (17) can be also extracted from the semiclassical characteristic equation describing the intersubband polariton modes supported by perfect-metal/QW/dielectric (ε_w)/perfect-metal structure.[33]] We should remember that the MCHOM takes into account only the resonant terms of the light-matter interaction. In other words, it is based on the rotating wave approximation (RWA). Therefore, it correctly describes the strong-coupling regime but it cannot describe the peculiar features of the ultrastrong coupling limit.[11]

Once the matrix elements $V_{n\kappa}$ are known, a $M\times M$ coupling Hamiltonian $\mathcal{H}$ can be constructed (see, e.g., Ref. 19). $M=N_{\mathrm{QW}}+N_{\mathrm{ph}}$, where N_{ph} is the number of the included photonic modes. (In the systems considered here practically only the two or three lowest photonic modes play a non-negligible role.) The diagonalization of this Hamiltonian gives information on the properties of the polariton modes supported by the system.[19,25] A large value of N_{QW} $(>10^2)$ substantially complicates the simulations. Fortunately, we have checked that the behavior of systems with a very large number of QWs is well modeled by the simplified system (described by the coupling Hamiltonian $\mathcal{H}_{\mathrm{appr}}$) with a relatively small number of the QWs (~10) provided that parameters d_{MQW}, $N_{\mathrm{QW}}\mathcal{N}_s$ as well the position of the MQW are unchanged.[19] Using $\mathcal{H}_{\mathrm{appr}}$ we have been able to reproduce essential properties of the dispersion relation presented in Fig. 4. To check the correctness of this simplification we have performed additional simulations based the TMF and the sheet model. Calculations are performed for the structure similar to those studied Dupont *et al.* They show that the above-mentioned reduction in the N_{QW} very weakly affects the angle-resolved absorption spectra provided that not only the parameters d_{MQW}, $N_{\mathrm{QW}}\mathcal{N}_s$ but also the ratio $f=L_{\mathrm{QW}}/L_{\mathrm{MQW}}$ or more precisely the parameters ϵ_{ii} (see Appendix A) are fixed. It is interesting to note that the formation of the central polariton mode (L_2), responsible for the appearance of the central peak in the $\lambda/2$ BMC, is predicted even by a very simplified the four-oscillator model ($M=4$). In this model the MQW is replaced by the two QWs (positioned at $z_1=\frac{1}{4}L_{\mathrm{MC}}$ and $z_2=\frac{3}{4}L_{\mathrm{MC}}$) and the two lowest photonic modes are included.

Below we show that a much more rigorous approach employing the concept of bright and dark intersubband states[6,18,19,23,24,26,28] can be successfully used for description of the intersubband polariton modes in BMCs. It allows for the derivation of simple analytical results for the polariton mode dispersion and the angle-resolved absorption spectra.

2. Introduction of bright and dark states

Let us denote the intersubband state supported by the κth QW by Ψ_κ. (The in-plane wave vector q_x will be omitted for simplicity). For further discussion it is convenient to introduce the following bases for the intersubband states supported by the whole MQW:

$$\mathcal{D}_\mu=\sum_{\kappa=1}^{N_{\mathrm{QW}}}C_\kappa^{(\mu)}\Psi_\kappa. \tag{18}$$

Physically, the $\mathcal{D}_\mu$'s represent intersubband states delocalized over the N_{QW} quantum wells according to specific coherent linear combinations of the original single-well intersubband states. For the so-called bright state ($\mu=1$) we take $C_\kappa^{(1)}=\mathbf{A}_1\mathcal{E}_1(z_\kappa)$ where $\mathbf{A}_1^{-2}=\Sigma_{\kappa=1}^{N_{\mathrm{QW}}}\mathcal{E}_1^2(z_\kappa)$. The remaining $N_{\mathrm{QW}}-1$ dark states are characterized by N_{QW}-component vectors $\mathbf{C}^{(\mu)}$ $(\mu=2\cdots N_{\mathrm{QW}})$, which can be taken orthogonal to the vector $\mathbf{C}^{(1)}$. In other words, the following relation is fulfilled:

$$\sum_{\kappa=1}^{N_{\mathrm{QW}}}C_\kappa^{(\mu)}C_\kappa^{(1)}=\delta_{\mu,1}. \tag{19}$$

Employing Eqs. (16) and (18) we find that the matrix element for excitation of the electronic state $\mathcal{D}_\mu$ by the c_n photonic mode can be written as[18]

$$\bar{V}_{n\mu}(k_x) \equiv \hat{V}_{n\mu} \sin\theta_n = V_{\max} \sum_{\kappa=1}^{N_{QW}} C_\kappa^{(\mu)} \mathcal{E}_n(z_\kappa) \sin\theta_n. \quad (20)$$

From the above relations one finds that $\hat{V}_{1\mu} = \mathbf{A}_1^{-1} V_{\max} \delta_{\mu,1}$. Thus, the ground photonic mode (c_1) couples only to the bright state $\mathcal{D}_1$. [The equivalent expression for $\mathcal{D}_1$ and $\hat{V}_{1\mu}$ results also from the diagonalization of the coupling Hamiltonian in which higher photonic modes ($c_{n>1}$) are not included.[25,26]] Thus, we can say that the radiative coupling rearranges the N_{QW} independent intersubband states into a single, bright state which is coupled to the c_1 mode and $N_{QW}-1$ dark states which do not interact with this mode. The factor $N_{QW}^{eff} = \mathbf{A}_1^{-2}$ can be treated as the effective number of QWs interacting with the ground cavity mode. It takes a maximal value ($N_{QW}^{eff} \cong N_{QW}$) when all QWs are located in the vicinity of the antinode.

As the first one we discuss the case of the $\lambda/2$ BMC ($d_{MQW} = L_{MC}$). Such systems usually contain a very large number of QWs uniformly distributed between the mirrors. Thus appropriate summations can be converted into integrations. Then, we find that $\mathbf{A}_n^{-2} = N_{QW}/2$ and

$$C_\kappa^{(\mu)} \cong (2/N_{QW})^{1/2} \mathcal{E}_\mu(z_\kappa). \quad (21)$$

Substituting the above relation into Eq. (20) one gets $\hat{V}_{n\mu} = \hat{V}_{nn}\delta_{\mu,n}$ where $\hat{V}_{nn} = \omega_p/2$ and $\omega_p^2 = 4\pi e^2 \mathcal{N}_s / m^* \varepsilon_w L_{MQW}$. It means that, in the case of the $\lambda/2$ BMC, the c_n photonic mode couples only to the $\mathcal{D}_{\mu=n}$ electronic mode. (The above findings are also valid in the case of the $\lambda/4$ BMC.) This result is fully equivalent to that obtained modeling the MQW by an effective medium [see Eqs. (A5) and (A6)] and using the round-trip quantization condition $k_z^{(MQW)} L_{MC} = n\pi$ with $n = 1,2,3,\ldots$.[6,34] (In the case of metallic mirrors[15,33] $n = 0,1,2,\ldots$.)

When the MQW is centrally positioned but $d_{MQW} < L_{MC}$ (or N_{QW} is relatively small) the selection rule $\mu = n$ should be replaced by the less restrictive "parity" selection rule $|\mu - n| = 0,2,4,\ldots$. Note that in the simplest case of two QWs ($\kappa = 1,2$) positioned symmetrically in the MC we get $\mathcal{D}_1 \equiv \mathcal{D}_S = (\Psi_1 + \Psi_2)/\sqrt{2}$ and $\mathcal{D}_2 \equiv \mathcal{D}_A = (\Psi_1 - \Psi_2)/\sqrt{2}$.[23] Let us assume that the above-mentioned QWs are positioned at $z_1 = \frac{1}{4} L_{MC}$ and $z_2 = \frac{3}{4} L_{MC}$ (or equivalently that the MQW contains only two QWs). Then one can check that the matrix elements $\hat{V}_{11}$ and $\hat{V}_{22}$ predicted by the four-oscillator model[19] are close to those obtained for the $\lambda/2$ BMC with $N_{QW} \gg 1$ but having the same value of the product $N_{QW}\mathcal{N}_s$. It explains why this model successfully captures the main effects induced by the coupling of the two lowest photonic modes with intersubband transitions.

In the case of the MC with an asymmetrically positioned MQW (or when one of the mirrors is metallic, such as in the $\lambda/4$ MBC) even the above-mentioned parity selection rule is violated. It is instructive to discuss the particular case when the MQW occupies the region $L_{MC}/2 < z < L_{MC}$ [see Fig. 2(b)]. Assuming that $N_{QW} \gg 1$ we get the following approximated expression for $C_\kappa^{(\mu)}$:

$$C_\kappa^{(\mu)} = (2/N_{QW})^{1/2} \mathcal{E}_{2\mu-1}(z_\kappa). \quad (22)$$

From Eqs. (20) and (22) one finds that $\hat{V}_{22}/\hat{V}_{11} \cong 0.5$ and $\hat{V}_{21}/\hat{V}_{11} \cong 0.85$. This result leads to the conclusion that the formation of the complex multimode polaritons containing the admixture of not one but two (or even more) electronic and photonic modes is, in principle, possible. [The similar conclusion results from the four-oscillator model in which the MQW is replaced by the two QWs (see Fig. 3 in Ref. 19).] However, we should remember that in the experimentally studied $\lambda/2$ MCs (with $d_{MQW} < L_{MC}$) the MQW is always centrally positioned to maximize $\Omega_{R_{res}}$. In such systems the reduction in the parameter $\Xi = d_{MQW}/L_{MC}$ leads to the dramatic decrease in the ratio $\hat{V}_{(\eta>1)\eta(\eta'>1)}/\hat{V}_{11}$. It implies that in the limit $\Xi \ll 1$ the effects connected with the presence of higher photonic modes can be safely neglected.

The results presented above indicate that in the case when the MQW occupies a large fraction of space between mirrors then not Ψ_κ but rather $\mathcal{D}_\mu$ states should be associated with independent (electronic) oscillators. The main advantage of this approach is connected with the fact that describing the coupling of intersubband transitions with photonic modes we can restrict (in the first approximation) to the diagonal approximation taking $\hat{V}_{n\mu} \cong \hat{V}_{nn}\delta_{\mu,n}$. In other words the main properties of the cavity polaritons supported by the BMC are captured assuming that the electronic [see Eq. (18)] and photonic modes having the same mode index (and the same in-plane wave vector) behavior as two-coupled harmonic oscillators. Below we discuss the main results predicted by this approximation.

3. Diagonal approximation

The coupling of the $\mathcal{D}_n$ and c_n modes leads to the formation of the upper $+n \equiv U_n$ and lower $-n \equiv L_n$ polariton branches. Their dispersion in the k_x-ω plane takes a well-known form (see Appendix C). The above branches are a coherent mixture of the c_n and $\mathcal{D}_n$ states whose fractions are given by Hopfield coefficients $\mathcal{X}_{\pm n}(k_x)$ and $\mathcal{C}_{\pm n}(k_x)$ (see Appendix C).

Using Eq. (13) we can transform the polariton dispersion relation (predicted by the two-oscillator model) from the k_x-ω plane to the φ-ω plane. Taking into account the dissipation we get (see Appendix C)

$$\tilde{\omega}_{\pm n}(\varphi) = \frac{\tilde{\omega}_{IT} + \tilde{\omega}_{c_n}(\varphi)}{2} \pm \frac{1}{2}\sqrt{\tilde{\delta}_n^2(\varphi) + 4[\bar{\Omega}_R^{(n)}]^2}, \quad (23)$$

where $\tilde{\omega}_{IT} = \omega_{IT} - i\gamma_{IT}$, $\tilde{\omega}_{c_n}(\varphi) = \omega_{c_n}(\varphi) - i\gamma_{c_n}(\varphi)$, $\omega_{c_n}(\varphi) = n\omega_\perp/\cos(\varphi)$, $\bar{\delta}_n(\varphi) = \omega_{c_n}(\varphi) - \omega_{IT}$, and $\bar{\Omega}_R^{(n)}(\varphi) = \hat{V}_{nn} \tan\varphi$. The quantity γ_{c_n} (γ_{IT}) is the decay rate of the c_n cavity mode (intersubband transitions). The resonant mode splitting predicted by Eq. (23) can be written (in the SCR) as $2\bar{\Omega}_{R_{res}}^{(n)} = 2\bar{\Omega}_R^{(n)}(\varphi_n^{res})$, where φ_n^{res} is defined by relation $\omega_{c_n}(\varphi_n^{res}) = \omega_{IT}$. As it was mentioned $\bar{\Omega}_{R_{res}}^{(n)}$ does not coincides with

Rabi splitting $\Omega_{R_{res}}^{(n)}$. In the systems considered here difference between ε_b, ε_s, and ε_w is small. It implies that the difference between θ_n^{res} and φ_n^{res} is also small. Neglecting this difference we get the following useful relation: $\Upsilon_n \equiv \bar{\Omega}_{R_{res}}^{(n)} / \Omega_{R_{res}}^{(n)} = 1/\cos\varphi_n^{res}$. Taking, like in the system studied by Dupont *et al.*,[2,14] $\varphi_1^{res} \cong 73°$ we get $\Upsilon_1 \cong 3.4$. Thus $\bar{\Omega}_{R_{res}}^{(1)}$ is usually several times larger than $\Omega_{R_{res}}^{(1)}$. It is a consequence of the fact that the external radiation propagating at the angle φ_1^{res} couples resonantly to the polariton branches with the wave vectors which substantially differ from k_1^{res} defined by relation $\omega_{c_1}(k_1^{res}) = \omega_{\mathrm{IT}}$. This implies that although the angular dependence of the U_1 and L_1 branches [predicted by Eq. (23)] takes the same form as that resulting from the two-coupled oscillator model, the polariton states associated with upper and lower peaks observed in angle-resolved spectra of the resonant MC do not contain the same fraction of the electronic and photonic components. We will return to this problem in Sec. IV.

In the diagonal approximation the expression for the absorption spectrum can be generally written as $A(\omega) = \Sigma_n A_n(\omega)$, where $A_n(\omega)$ the absorption connected with the branches $+n$ and $-n$. The application of the input-output formalism makes it possible to calculate $A_n(\omega)$ (see Appendix C). The expression for $A_n(\omega)$, at fixed φ, can be approximated by

$$A_n(\omega) = \frac{4\gamma_{c_n}^{rad}\{[\bar{\Omega}_R^{(n)}]^2\gamma_{\mathrm{IT}} + \gamma_{c_n}^{abs}[(\omega-\omega_{\mathrm{IT}})^2 + \gamma_{\mathrm{IT}}^2]\}}{|[\tilde{\omega}_{c_n}(\varphi)-\omega](\tilde{\omega}_{\mathrm{IT}}-\omega) - [\bar{\Omega}_R^{(n)}(\varphi)]^2|^2}. \tag{24}$$

where $\gamma_{c_n}^{rad} = \gamma_{c_n}^{abs} + \gamma_{c_n}^{rad}$, $\gamma_{c_n}^{rad}(\gamma_{c_n}^{abs})$ is radiative (absorptive) cavity mode decay.

In Appendix D we show that, in the case of the $\lambda/2$ BMC, the equivalent formula can be obtained employing a standard multibeam interference analysis (and the RWA). This analysis also indicates that incorporating the mirror losses into $\gamma_{c_n}^{abs}$ has a justification. In other words we can assume that the decay rate $\gamma_{c_n}^{rad}$ ($\gamma_{c_n}^{abs}$), appearing in the above formula obeys the relation given by Eq. (D5) [Eq. (D6)].

At ω close to $\omega'_{\pm n}$, the resonant contribution connected with the branch $\pm n$ reduces (in the SCR) to the same form as that predicted by the semiclassical approach [see Eq. (14)]. It can be written as

$$A_{\pm n}(\omega) \cong \mathcal{A}_{\pm n}\frac{1}{1+[\omega-\omega'_{\pm n}(\varphi)]^2/\gamma_{\pm n}^2} \tag{25}$$

with

$$\mathcal{A}_{\pm n} = 4\gamma_{\pm n}^{rad}\gamma_{\pm n}^{abs}/\gamma_{\pm n}^2, \tag{26}$$

where $\gamma_{\pm n} = \gamma_{\pm n}^{rad} + \gamma_{\pm n}^{abs}$, $\gamma_{\pm n}^{rad} = \bar{\mathcal{C}}_{\pm n}^2\gamma_{c_n}$, and $\gamma_{\pm n}^{abs} = \bar{\mathcal{X}}_{\pm n}^2\gamma_{\mathrm{IT}} + \bar{\mathcal{C}}_{\pm n}^2\gamma_{c_n}^{abs}$. $\bar{\mathcal{C}}_{\pm n}$ and $\bar{\mathcal{X}}_{\pm n}$ are modified Hopfield coefficients (see Appendix C).

From Eq. (26) we find that in the resonant case ($\varphi = \varphi_1^{res}$) the expression for the height of the peaks, associated with L_1 and U_1 branches reduces to the form

$$\mathcal{A}_{+1} = \mathcal{A}_{-1} = \frac{4\gamma_{c_1}^{*rad}(\gamma_{c_1}^{*abs}+\gamma_{\mathrm{IT}})}{(\gamma_{c_1}^{*rad}+\gamma_{c_1}^{*abs}+\gamma_{\mathrm{IT}})^2}, \tag{27}$$

where $\gamma_{c_1}^{*rad} = \gamma_{c_1}^{rad}(\varphi_1^{res})$ and $\gamma_{c_1}^{*abs} = \gamma_{c_1}^{rad}(\varphi_1^{res})$.

The depth of the absorptance splitting at its lowest point, i.e., at $\omega = \omega_{\mathrm{IT}}$ is given by

$$A_{\pm 1}^{\min} = \frac{4\gamma_{c_1}^{*rad}\gamma_{\mathrm{IT}}[\bar{\Omega}_{R_{res}}^2 + \gamma_{c_1}^{*abs}\gamma_{\mathrm{IT}}]}{(\gamma_{\mathrm{IT}}\gamma_{c_1}^* + \bar{\Omega}_{R_{res}}^2)^2} \approx \frac{4\gamma_{c_1}^{*rad}\gamma_{\mathrm{IT}}}{\bar{\Omega}_{R_{res}}^2}. \tag{28}$$

Moreover, when φ is close to φ_1^{res} and $[2\bar{\Omega}_R^{(n)}(\varphi_1^{res})/\bar{\delta}_n(\varphi_1^{res})]^2 \ll 1$ then the following useful relations (devoted to the $L_{n>1}$ branches) result from Eqs. (23), (25), and (26):

$$\omega'_{L_n} = \omega_{\mathrm{IT}}\left\{1 - \frac{1}{n-1}\left[\frac{\bar{\Omega}_R^{(n)}(\varphi_1^{res})}{\omega_{\mathrm{IT}}}\right]^2\right\} \tag{29}$$

and

$$\mathcal{A}_{L_n} = \frac{4}{(n-1)^2}\left[\frac{\bar{\Omega}_R^{(n)}(\varphi_1^{res})}{\omega_{\mathrm{IT}}}\right]^2\frac{\gamma_{c_1}^{*rad}}{\gamma_{\mathrm{IT}}}. \tag{30}$$

In obtaining Eq. (30) we have assumed that $\gamma_{\mathrm{IT}} \gtrsim \gamma_{c_n}^{rad} \gtrsim \gamma_{c_n}^{abs}$.

III. DESCRIPTION OF SAMPLES AND UNCOUPLED PHOTONIC MODES

The numerical calculations reported in this paper are performed for the three systems (see Fig. 1). The first one is the $\lambda/2$ BMC presented in Fig. 1(a). To facilitate the comparison with results presented in the literature we assume that this structure is similar to those studied experimentally by Dupont *et al.*[2] and theoretically in our previous paper.[6] It is grown on a GaAs semi-insulating substrate ($\varepsilon_{\mathrm{GaAs}}$) and consists of a 140-repeat ($N_{\mathrm{QW}}=140$) MQW embedded between a 0.4-μm-thick n^+ GaAs top layer (back mirror) and 0.8-μm-thick n^+ GaAs bottom layer (coupling mirror) with the doping concentration $N_D = 2\times10^{18}$ cm^{-3}. The cladding medium is Au. The period of the MQW consists of a 60-Å GaAs QW and a 290-Å $Al_{0.21}Ga_{0.79}As$ barrier. The QW is treated as a two-subband system with: $\hbar\omega_{\mathrm{IT}} = 114$ meV, $\mathcal{N}_s = 2\times10^{11}$ cm^{-2}, and $\hbar\gamma_{\mathrm{IT}} = 3.1$ meV. The above parameters are relevant to the system studied by Dupont *et al.*[14] (The numerical simulations reported in our previous paper[6] have been performed for the parameters $\mathcal{N}_s = 2\times10^{10}$ cm^{-2} and $\hbar\gamma_{\mathrm{IT}} = 1.1$ meV relevant to the system studied in Ref. 2.) To get additional information on the role of the higher photonic modes in the formation of the intersubband cavity polaritons we also discuss a system which differs from the above-mentioned one only by (i) the smaller value of the $Al_{0.21}Ga_{0.79}As$ barrier thickness (not 290 Å but 115 Å) and (ii) the presence (between the MQW and the coupling mirror) of the additional $Al_{0.21}Ga_{0.79}As$ spacing layer with thickness $d_{spac} = L_{\mathrm{MC}}/2$ [see Fig. 1(b)]. We call it the $\lambda/2$ "half" BMC.

The giant mode splitting was also observed in the $\lambda/4$ BMC where the confinement of the radiation is realized by

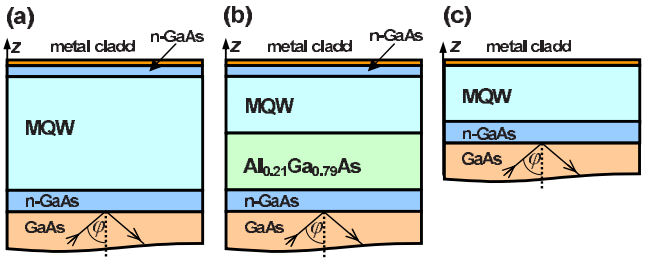

FIG. 1. (Color online) Diagrams illustrating schematically the geometry of the three structures discussed in the paper: (a) the $\lambda/2$ BMC, (b) the $\lambda/2$ half BMC, and (c) the $\lambda/4$ BMC.

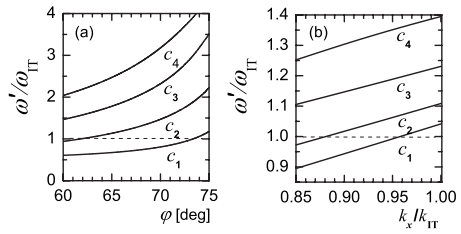

FIG. 2. The real part of the frequencies of the four lowest photonic modes supported by the $\lambda/2$ BMC described in the text as a function of (a) φ and (b) k_x. $k_{IT}=\varepsilon_{GaAs}^{1/2}\omega_{IT}/c$.

sandwiching the optically active material between a bottom dielectric mirror and a top metallic mirror.[5,9] For this reason we have also performed appropriate simulations for a $\lambda/4$ BMC [see Fig. 1(c)]. It differs from the previously described $\lambda/2$ BMC [see Fig. 1(a)] by (i) the reduction in the N_{QW} from 140 to 70 and (ii) replacement of the upper dielectric-metallic mirror by the purely metallic (Au) mirror.

Now we briefly discuss the main properties of the uncoupled photonic modes in the systems shown schematically in Fig. 1. The photonic modes supported by the $\lambda/2$ BMC and the half $\lambda/2$ BMC can modeled, in the first approximation, by the Fabry-Perot MC with nearly perfect dielectric mirrors. It implies that the photonic modes in these systems can be divided into even ($n=1,3,\ldots$) and odd ($n=2,4,\ldots$) parity in E_z (with respect to the center of the cavity) photonic modes (see Fig. 1 in Ref. 14). In the case of the $\lambda/4$ BMC [see Fig. 1(c)] the simplified model with the metallic back mirror and the dielectric coupling mirror can be used. Employing this fact, one finds that the photonic modes supported by the above-mentioned system practically coincide with even-parity photonic modes supported by the $\lambda/2$ BMC. Due to that, the photonic modes in the $\lambda/4$ BMC will be denoted by the mode index $n=1,3,5,\ldots$ instead of $n=1,2,3,\ldots$.

Figure 2(a) presents the φ dependence of the four lowest photonic modes c_n ($n=1,2,3,4$) supported by the $\lambda/2$ BMC obtained with the help of the TMF. We find that the resonant angle φ_1^{res} (φ_2^{res}), at which $\omega_{c_1}(\varphi)\equiv \mathrm{Re}\tilde{\omega}_{c_1}(\varphi)$ [$\omega_{c_2}(\varphi)\equiv \mathrm{Re}\tilde{\omega}_{c_2}(\varphi)$] coincides with ω_{IT}, is close to 73.40° (61.87°). These values are in good agreement with those reported by Dupont *et al.*[2,14] In the case of resonant structure ($\varphi=\varphi_1^{res}$) the separation between each two adjacent photonic modes is close to ω_{IT}. This fact is probably the main reason why a single mode cavity approximation is commonly used (even in the papers employing a full quantum-mechanical treatment[5,11,12,35]).

It is worth noting that the behavior of the photonic modes in the considered systems is only semiquantatively described by the simplified model (with nearly perfect dielectric mirrors). For example, this model predicts that $\omega_{c_n}(\varphi)=n\omega_{c_1}(\varphi)$ and $\omega_{c_n}(\varphi)\propto \cos^{-1}(\varphi)$. From Fig. 2 one finds that the adjacent mode separation $\bar{\Delta}_{(n+1)n}(\varphi)=\omega_{c_{n+1}}(\varphi)-\omega_{c_n}(\varphi)$ does not coincide with $\omega_{c_1}(\varphi)$. In the most interesting case, $\varphi=\varphi_1^{res}$, the separation between the two lowest modes takes the value close to 0.9 ω_{IT}. It is also easy to see (particularly in the case of the lowest mode) that the φ dependence of the mode frequency is not well approximated by $\cos^{-1}(\varphi)$. The above-mentioned deviation is mainly due to the fact that the penetrations of the cavity modes into the mirrors (the phase change at the reflection) strongly depends on ω (and φ). The numerical simulations (not presented here) fully support the above suggestion.

As one can expect the cavity mode relaxation rate contains the radiative and absorptive contributions $\gamma_{c_n}=\gamma_{c_n}^{rad}+\gamma_{c_n}^{abs}$. The latter contribution is connected mainly with the absorptive losses in the mirrors. In the systems considered here it plays a nonnegligible role (i.e., $\gamma_{c_n}^{abs}$ is comparable with $\gamma_{c_n}^{rad}$) only in the case of the ground mode. For example, from Fig. 1b in Ref. 6 we find that in the case of the resonant $\lambda/2$ BMC $\gamma_{c_1}\approx 6.5$ meV and $\gamma_{c_1}^{rad}\approx 3.8$ meV. This figure also shows that, in contrast to the simplified model, the ratio $\gamma_{c_n}^{rad}/\omega_{c_1}$ increases with increasing n and φ. It is obvious that this fact can be also associated with the dispersivity of the mirrors. The quality factors $Q_n(=\omega_{c_n}/2\gamma_{c_n})$ are rather small. Due to the above-mentioned facts, they decrease very fast with the increase in the mode index and φ. For example, in the case of the resonant $\lambda/2$ BMC (and the $\lambda/2$ half BMC) the TMF gives $Q_1\simeq 10$, $Q_2\simeq 5$, and $Q_3\simeq 3$. It is worth noting that, in qualitative agreement with Eq. (D4), the numerical values of the quality factors in the $\lambda/4$ BMC (with back metallic mirror) are about two times smaller than in the $\lambda/2$ BMC.

As it was mentioned in Sec. II the knowledge of the behavior of the photonic modes in the k_x-ω plane is required for the correct description of the coupling between the photonic and intersubband transitions. For this reason in Fig. 2(b) we additionally present the dispersion curves of the cavity modes extracted from Fig. 2(a) employing fact that when $|\omega_\iota''|\ll\omega_\iota'$ then Eq. (13) can be simplified to the form

$$\sin\varphi\approx k_x c/\omega_\iota'\sqrt{\varepsilon_s}. \tag{31}$$

We find that the resonant wave vector k_1^{res} (k_2^{res}) at which $\omega_{c_1}(k_x)$ [$\omega_{c_2}(k_x)$] coincides with ω_{IT}, is close to 0.96 k_{IT} (0.88 k_{IT}) where $k_{IT}=\varepsilon_{GaAs}^{1/2}\omega_{IT}/c$. It can be easily observed that (at large φ) the mode separation in the k_x-ω plane, $\Delta_{jn}(k_x)=\omega_{c_j}(k_x)-\omega_{c_n}(k_x)$, is much smaller than in the φ-ω plane. From Fig. 2(a) we find that $\Delta_{21}^*\equiv\Delta_{21}(k_1^{res})$ takes the value of $\approx 0.07\omega_{IT}$. Note that due to the penetration of the cavity modes into the mirrors this value is noticeably smaller than that predicted by the model with nearly perfect mirrors. For

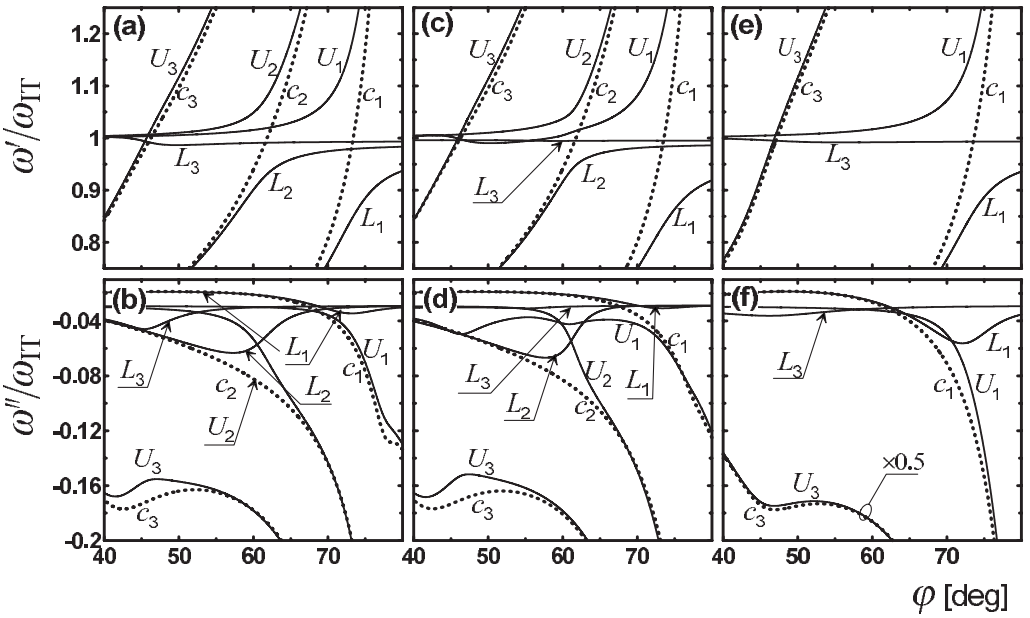

FIG. 3. The real part (upper panels) and imaginary part (lower panels) of the frequencies of the modes c_i, U_i, and L_i (with $i \leq 3$) supported by [(a) and (b)] the $\lambda/2$ BMC, [(c) and (d)] the $\lambda/2$ half BMC, and [(e) and (f)] the $\lambda/4$ BMC as a function of φ. The solid (dotted) curves correspond to the polaritonic (photonic) modes.

example, when $\varphi_1^{res} \gtrsim 60°$ the above model leads to the following relation: $\Delta_{21}^*/\omega_{IT} \cong 1.5 \cos^2(\varphi_1^{res})$. Taking $\varphi_1^{res}=73.4°$ we get $\Delta_{21}^*/\omega_{IT} \cong 0.12$. The above estimations (see also Fig. 4) indicate that in the system studied by Dupont *et al.*[14] $\Omega_R^{(2)}(k_1^{res})$ is comparable with Δ_{21}^*. It leads to the conclusion that the formation of the L_2 branch should be taken into account in the correct interpretation of the angle-resolved absorption spectra (at $\varphi \simeq \varphi_1^{res}$). Numerical simulations presented in the next section fully support the above suggestion.

IV. NUMERICAL RESULTS AND DISCUSSION

Figure 3 displays the φ dependence of the polariton modes obtained solving numerically the dispersion Eq. (12) [see also Eq. (13)] for the systems schematically shown in Fig. 1. Figure 4 displays the k_x dependence of the polariton modes extracted from Fig. 3 with the help of Eq. (31). Only a few upper and lower branches ($n \leq 3$), which are mainly responsible for the features observed in the angle-resolved absorption spectra, are presented.

The inspection of the presented results shows that the behavior of the polariton modes in all of the considered systems is qualitatively similar. It is interesting that the k_x and φ dependence of the upper (U_n) and lower (L_n) branches can be qualitatively modeled by the two strongly coupled oscillators not only for $n=1$ (like in the system studied in our previous paper[6]) but also for $n=2$. It is due to large electron concentrations and consequently large Rabi splitting in the systems considered here. Note, however, that now the two-oscillator model does not work so well as in Ref. 6. For example, the relation $\omega'_{U_1}(\varphi_1^{res})+\omega'_{L_1}(\varphi_1^{res})=2\omega_{IT}$ resulting from the two-oscillator model is fulfilled only with the accuracy of $\sim 10\%$. Additionally, the heights of the two main peaks are different. It is also easy to see that the anticrossing of the curves ω'_{U_1} and ω'_{L_1}, at φ close to φ_1^{res}, is not accompanied by the crossing of the curves ω''_{U_1} and ω''_{L_1}. These effects can be connected with a strong dispersivity of the cavity mirrors which results mainly from the dispersivity of the dielectric constant of the n^+ GaAs layers. Note that in the MCHOM the ω dependence of the amplitude reflection coefficients of the mirrors is not considered. Simulations show that this dependence very strongly affects the behavior of the lowest polariton branches (and the angle-resolved absorption spectra) in the systems studied by Dupont *et al.*[14] and Sapienza *et al.*[9] A detailed discussion of the above-mentioned problem will be presented in a separate paper.

Some small qualitative difference in the behavior of the U_1 branches in the $\lambda/2$ BMC and $\lambda/2$ half BMC is observed at $\varphi \approx \varphi_2^{res}$. It seems that this difference can be associated with the presence (due to the lower symmetry of the $\lambda/2$ half BMC) of the nondiagonal coupling between c_2 and $\mathcal{D}_1$ modes. As it has been mentioned, this coupling enables the formation of the multimode polariton states with the dispersion deviating from that obtained in the diagonal limit.

The results presented in Figs. 3 and 4 support the fact predicted by the two-oscillator model that in the systems with $\varphi_1^{res} \approx 70°$ the Rabi frequency ($\Omega_{R_{res}}$) is about three times smaller than the mode splitting in the φ-ω plane ($\bar{\Omega}_{R_{res}}$). As it was mentioned, it is a consequence of the fact that polariton modes associated with the two main peaks correspond to the different values of $k_x=\bar{k}_{\pm 1}^{res}$. They are defined by relations $\omega'_{\pm 1}(\bar{k}_{\pm 1}^{res})=\omega'_{\pm 1}(\varphi_1^{res})$. Thus we can see that in spite of the fact that the behavior of the L_1 and U_1 branches on the φ-ω plane is well modeled by the two-oscillator model, the above branches do not contain the same fraction of the electronic and photonic components at the anticrossing point, i.e., when φ is very close to φ_1^{res}. Equivalently, we can say that the fraction of the electronic (photo-

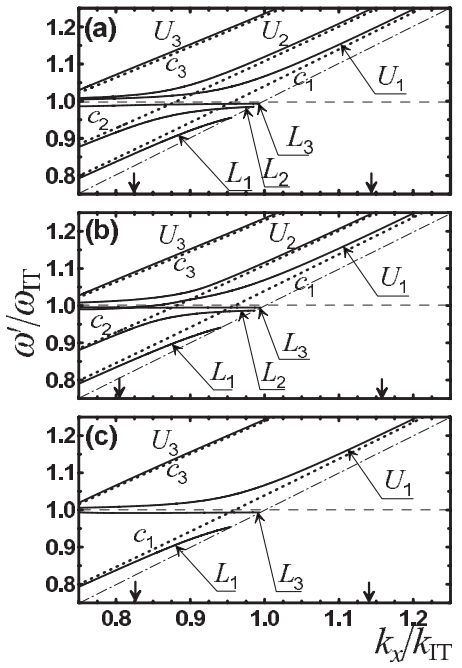

FIG. 4. The real part of the frequencies of the modes c_i, U_i, and L_i (with $i \leq 3$) supported by (a) the $\lambda/2$ BMC, (b) the $\lambda/2$ half BMC, and (c) the $\lambda/4$ BMC as a function of k_x. The dot-dashed line is defined by relation $k_x = \varepsilon_{GaAs}^{1/2} K$. The half space located below this line is not accessible by reflectance measurement. In the above-mentioned region the polariton modes have nonradiative character. The vertical arrows are positioned at $k_x = \bar{k}_{\pm 1}^{res}$ such that $\omega'_{L_1}(\bar{k}_{-1}^{res}) = \omega'_{L_1}(\varphi_1^{res})$ and $\omega'_{U_1}(\bar{k}_{+1}^{res}) = \omega'_{U_1}(\varphi_1^{res})$. The solid (dotted) curves correspond to the polaritonic (photonic) modes.

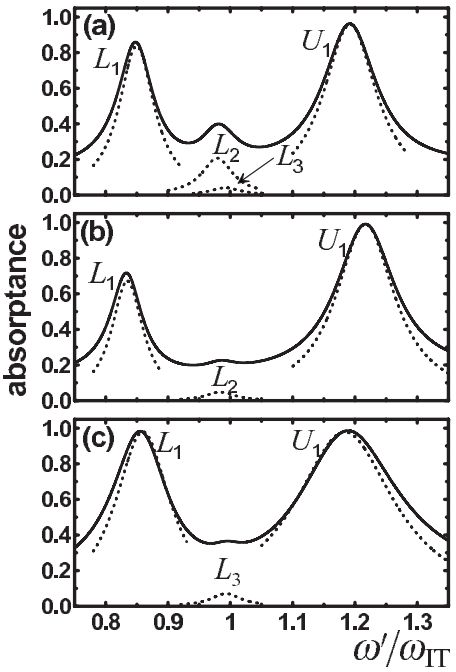

FIG. 5. The spectral dependence of the absorptance of (a) the $\lambda/2$ BMC, (b) the $\lambda/2$ half BMC, and (c) the $\lambda/4$ BMC at $\varphi = \varphi_1^{res}$. The solid (dotted) curves are obtained employing Eq. (11) [Eq. (14)].

nic) component is not quantified correctly by the modified Hopfield coefficient $\bar{\mathcal{X}}_{\pm 1}$ ($\bar{\mathcal{C}}_{\pm 1}$). When φ_1^{res} is sufficiently large the expression for the parameters $\mathcal{F}_1(\bar{k}_{\pm 1}^{res})$, controlling the composition of the above-mentioned polariton branches (at $k_x = \bar{k}_{\pm}^{res}$), can be approximated by (see Appendix C),

$$\mathcal{F}_1(\bar{k}_{\pm 1}^{res}) \cong \frac{2\bar{\Omega}_{R_{res}}\Omega_{R_{res}}}{\bar{\Omega}_{R_{res}}^2 - \Omega_{R_{res}}^2} = \frac{2\cos(\varphi_1^{res})}{\sin^2(\varphi_1^{res})}. \tag{32}$$

Taking $\varphi_1^{res} = 73.4°$ we get (in agreement with the numerical results displayed in Figs. 3 and 4) that $\mathcal{F}_1(\bar{k}_{\pm 1}^{res}) \approx 0.62$. It implies that $\mathcal{X}_{\pm 1}^2(\bar{k}_{\pm 1}^{res}) \approx 0.072$. Thus the polaritonic modes responsible for the two main peaks in considered here structures have practically photonic character. It is remarkable that, in the limit considered here, the numerical value of $\mathcal{F}_1(\bar{k}_{\pm 1}^{res})$ (and consequently the composition of the branches) is controlled mainly by φ_1^{res}. More precisely, the admixture of the electronic component decreases with increasing φ_1^{res}.

In a similar way one can check that the L_2 branch, responsible for the central peak, has mainly electronic character $\mathcal{X}_{L_2}^2(k_1^{res}) \gg \mathcal{C}_{L_2}^2(k_1^{res})$ at $\varphi \gtrsim \varphi_1^{res}$. The admixture of the photonic component c_2 increases very fast with the increasing ratio $\Omega_R^{(2)}/\omega_{IT}$.

Figure 5 illustrates the fact that all three peaks, predicted by the TMF, are well reproduced by resonant contributions of the lowest order polariton branches [see Eq. (14)]. It is also interesting to note that the approximated expressions obtained in the framework of the two-oscillator model [see Eqs. (26)–(30)] reproduce the main features of the angle-resolved absorption spectra very well. For example, a small asymmetry of the central peak of the $\lambda/2$ BMC observed by Dupont *et al.*[14] can be probably associated with the fact that the central peak is assigned not to one but at least two central polariton branches, L_2 and L_3. From Eq. (29) [see also Fig. 3] one finds that ω'_{L_2} is slightly smaller than ω'_{L_3}. Moreover, Eq. (30), in a qualitative agreement with the single-pole approximation [see Eq. (15), predicts a dominant contribution of the branche L_2 to the central peak]. Unfortunately, the smallness of the splitting makes it impossible to resolve states L_2 and L_3 in the absorption spectrum. We have checked numerically, using the TMF, that in accordance with simplified Eq. (30) the visibility of the central peak increases with the increase in the Rabi splitting (more precisely $\mathcal{N}_s$) and the decrease in the relaxation rate γ_{IT}. This finding is in agreement with the experimental results reported by Dupont *et al.*[2,14]

Although in all three samples the splitting between the two main peaks is nearly the same, a substantial reduction in the central peak height is observed in the $\lambda/2$ half BMC as well as in the $\lambda/4$ BMC. In the latter case the reduction is associated with the previously mentioned fact that the $\lambda/4$ BMC does not support photonic modes corresponding to the c_2 mode of the $\lambda/2$ BMC. Consequently, the formation of a central peak in the above-mentioned structure is connected with the coupling of c_3 and $\mathcal{D}_3$ modes. Due to that the frequency mismatch is larger (and consequently, the coupling

efficiency is smaller) than in the case of the c_2 and $\mathcal{D}_2$ modes.

The reduction in the central peak height in the case of the $\lambda/2$ half BMC results from the reduction in the overlap between the c_2 and $\mathcal{D}_2$ modes. This overlap is controlled by factor $\hat{V}_{22}$. Estimations based on Eqs. (20), (22), and (30) indicate that in the $\lambda/2$ half BMC the above-mentioned factor and consequently the height of the central peak is about two times smaller than in the $\lambda/2$ BMC.

We should remember that the theoretical results obtained in this paper are based on a number of approximations, most notably the omission of the statistic disorder in the systems or more precisely, the inhomogeneous broadening of the intersubband transitions. Unfortunately, finding polariton states in disordered planar microcavities is a difficult task, which we are not attempting in this paper. In the systems studied by Dupont *et al.*[2,14] the disorder is expected to play a perturbative role. However, in the case of the electroluminescent devices based on the intersubband cavity polaritons the situation is more complex. It is connected with the fact that in the above-mentioned systems the optically active materials (the quantum cascade structures) are much more strongly disordered than typical MQW systems. Stimulated by the above-mentioned fact we will qualitatively discuss the role of the disorder on the formation of the central intersubband polariton modes and their manifestations in the angle-resolved absorption spectra of MQW-MC systems. For very rough estimation we can assume (like in the case of the excitonic polaritons[35]) that the disorder leads only to the inhomogeneous distribution of the intersubband frequencies, i.e., the frequencies of the electronic oscillators are not the same. In this case a standard MCHOM (Refs. 23–26 and 35) predicts the formation of additional centrally positioned polariton modes (and consequently the inhomogeneously broadened central peak) even in the single cavity mode approximation. Employing, like in Refs. 23 and 24, the three-oscillator model (the two QWs and the ground photonic mode) one finds that the admixture of the photonic component in the central polariton mode is controlled by the ratio $\mathcal{R}_{\mathrm{inh}}$ =(inhomogeneous broadening)/(Rabi splitting). The above results are consistent with those predicted by a more rigorous microscopic approach[28] in which the disorder induced coupling between the bright and dark excitonic states and the strong light-matter coupling are treated on equal footing. At this point it is interesting to note that (when φ is close to φ_1^{res} and the ratio $\mathcal{R}_{\mathrm{inh}}$ is small) the width of two main peaks (but not the central one) is practically controlled by homogeneous broadening.[26] We suppose that the mechanism connected with inhomogeneous broadening may play a important role in the formation of small central peak structure observed recently in $\lambda/4$ MC with embedded quantum cascade structure.[36] It is connected with the fact that due to larger cavity mode separation, in the above-mentioned systems, the presence of the higher cavity modes plays a less important role than in the $\lambda/2$ systems (see Fig. 5).

Up to now we have discussed the influence of the central polariton mode formation on the angle-resolved absorption spectra. However, recent electroluminescence experiments in MC-quantum cascade devices show that it is possible to obtain intersubband cavity polariton emission after resonant electrical excitation. The quantum theory of electron tunneling into intersubband polariton states developed by De Liberato and Ciuti[11] indicates that quantum efficiency of the electroluminescence takes largest values when electrons are injected into polariton states having large admixture of the photonic component. Thus one can expect that the formation of the central polariton modes, with small admixture of the photonic component, can also lead to the appearance of an additional small central peak in the electroluminescence spectra. This suggestion is consistent with recent experimental findings.[36] Moreover, it is reasonable to expect that due to the electronic character of the central polariton modes they may play a nonperturbative role in the electron transport.[11] We would like also to stress that, the mixing between the bright and dark intersubband states induced by the disorder or/and coupling with higher photonic modes (more exactly the formation of the multimode branches), may affect substantially all polariton relaxation processes.[19,24,28]

V. CONCLUDING REMARKS

We have discussed, employing the semiclassical approach and the MCHOM (supplemented by the input-output formalism), the formation and properties of intersubband cavity polariton modes. Special attention has been paid to the role of the higher photonic modes. We have shown, introducing the concept of the bright and dark intersubband states, that higher order photonic modes play an important role when (i) the MQW occupies a large fraction of the space between the cavity mirrors and (ii) the Rabi frequency $\Omega_{R_{res}}$ is comparable or larger than the MC mode separation in the k_x-ω plane. The coupling of the above-mentioned modes with the dark states leads then to the formation of higher photonic modes manifested as a strong central peak in the angle-resolved reflection-absorption spectra. Moreover, when the appropriate conditions are fulfilled the formation of complex multimode polariton branches is also possible.

ACKNOWLEDGMENTS

The work of M.Z. was partially supported by MNiSzW under Grant No. N202 109 32/2854, 2007–2009.

APPENDIX A: EFFECTIVE MEDIUM APPROXIMATION

The calculation of $\mathbf{L}^{\mathrm{QW}}$ (and consequently $\mathbf{T}^{\mathrm{MQW}}$) requires, in general, the solution of the Maxwell equations using a nonlocal susceptibility of the QW evaluated by linear-response theory, which incorporates the microscopic details of the electron wave functions of the initial and final states.[3,4,31] Fortunately, for the realistic value of the QW parameters it is reasonable to assume that the optical response connected with intersubband transitions is not sensitive to the actual distribution of the normal current density $j_z(z,\omega)$ induced (in the QW region) by the normal component of the external electric field E_z^{ext} but rather depends only on the total surface current $j_z^{\mathrm{2D}}(\omega)=\int_{-L_{\mathrm{QW}}/2}^{L_{\mathrm{QW}}/2} dz j_z(z,\omega)$. (We assume that the z dependence of E_z^{ext} in the region occupied by the QW

$|z|<L_{QW}/2$ is negligibly small.) In the above-mentioned approximation the electrons in the QW behave as a 2D sheet (located in the middle of the QW, i.e., at $z=0$) characterized by the modified surface conductivity defined by relation $\tilde{\sigma}_{zz}^{2D}(\omega)=j_z^{2D}(\omega)/E_z^{ext}(z=0)$. Note that this conductivity describes the (nonretarded) collective intersubband response of the electrons to the uniform external electric field $\mathbf{E}^{ext}(t)=\mathbf{e}_z E_z^{ext} e^{-i\omega t}$ not to the total electric field $\mathbf{E}$.[22,37]

In the case of the two parabolic subbands (lower subband $|1\rangle$ and upper subband $|2\rangle$) the expression for $\tilde{\sigma}_{zz}^{2D}(\omega)$, resulting from the local-density approximation (LDA), takes (in the long-wavelength limit) the form[37]

$$\tilde{\sigma}_{zz}^{2D}(\omega)=\frac{\Delta N_s e^2 f_{21}}{m^*}\frac{-i\omega}{\tilde{\omega}_{21}^2-\omega^2-i2\omega\gamma_{IT}}, \tag{A1}$$

where $\tilde{\omega}_{21}\equiv\omega_{IT}$ is the intersubband transition frequency. Due to the depolarization and excitonlike effects this frequency is slightly larger than the intersubband spacing ω_{21}. (Equivalently, we can say that ω_{IT} corresponds to the frequency of the intersubband plasmon, i.e., the collective intersubband oscillation due to the Coulomb interaction between electrons.) $f_{12}=2m^*\omega_{21}z_{21}^2/\hbar$ is the oscillator strength connected with the intersubband transitions ($f_{12}\approx 1$), γ_{IT} is the phenomenological dephasing rate connected with intersubband transitions, $\Delta N_s=N_s^{(1)}-N_s^{(2)}$, $N_s^{(\zeta)}$ is the surface electron concentration in ζth subband and finally, e and m^* are the charge and effective mass of the electron, respectively. In further discussion we restrict ourselves to the case when only ground subband is occupied ($\Delta N_s=N_s^{(1)}$) and neglect the intrasubband transitions. Note that in the systems with nonequilibrium inverse population ΔN_s is negative. [The properties of the eigenmodes of an idealized MC ($\gamma_{IT}=\gamma_{c_n}=0$) with $\Delta N_s<0$ have been discussed by Pereira[34] (see also Ref. 38)].

The QW transfer matrix predicted by the sheet model takes the following form:

$$\mathbf{L}^{QW}=\mathbf{L}(\beta_w/2)\mathbf{I}^{2D}\mathbf{L}(\beta_w/2), \tag{A2}$$

where matrix $\mathbf{I}^{2D}$ can be written in the terms of the reflection coefficient $r^{2D}[=(\Lambda_{QW}/2)/(1+\Lambda_{QW}/2)]$ and the transmission coefficient $t^{2D}[=1/(1+\Lambda_{QW}/2)]$ of the sheet as[22]

$$\mathbf{I}^{2D}=\frac{1}{t^{2D}}\begin{bmatrix}1 & -r^{2D}\\ r^{2D} & (t^{2D})^2-(r^{2D})^2\end{bmatrix}, \tag{A3}$$

where

$$\Lambda_{QW}=(4\pi/c\sqrt{\varepsilon_w})\tilde{\sigma}_{zz}^{2D}(\omega)\tan(\varphi_w)\sin(\varphi_w) \tag{A4}$$

with $\varphi_w=\arcsin[(\varepsilon_s/\varepsilon_w)^{1/2}\sin\varphi]$.

It is reasonable to expect that the above-mentioned sheet model should work well even when we go, like in Refs. 30 and 34, beyond the LDA and/or parabolic approximation. Another advantage of the sheet model is the possibility of the inclusion of the saturation of the intersubband transitions employing an approach described in our previous paper.[39] This problem will be the subject of our future papers.

Once the elements of the matrix $\mathbf{I}^{2D}$ are known the transfer matrix through the MQW can be calculated numerically. Nevertheless for our purpose it is much more convenient to choose a simplified approach developed in Ref. 22. It is based on the assumption that when the period of the MQW is much smaller than the wavelength of the optical field. (This simplifying assumption is reasonable in the case of the lowest order cavity modes.) Then we can model the MQW by an effective uniform uniaxial medium (slab). Standard boundary conditions require E_x (E_z) and D_z (D_x) to be continuous (discontinuous) at the interfaces. [$\mathbf{D}=\varepsilon(z)\mathbf{E}(z,\omega)+(i4\pi/\omega)\mathbf{j}(z,\omega)$ and $\varepsilon(z)$ is the background dielectric constant at point z]. Thus E_z and D_x must be suitably averaged over the period of the MQW to obtain its dielectric response when it is viewed as an effective medium. Performing appropriate manipulations we get the following general expressions for the components of the diagonal effective dielectric tensor $\varepsilon(\omega)$ (for details see Refs. 22 and 31):

$$\varepsilon_{\alpha\alpha}(\omega)\equiv\langle D_x\rangle/E_x=\epsilon_{xx}\quad\alpha=x,y, \tag{A5}$$

$$\varepsilon_{zz}^{-1}(\omega)\equiv\langle E_z\rangle/D_z=\epsilon_{zz}^{-1}-\Delta\varepsilon_{zz}(\omega)/\varepsilon_w^2, \tag{A6}$$

where $\langle\ \rangle$ denotes the spatial averaging over the MQW period, $\Delta\varepsilon_{zz}(\omega)=i4\pi\tilde{\sigma}_{zz}^{2D}(\omega)/\omega L_{MQW}$, $\epsilon_{xx}=(1-f)\varepsilon_b+f\varepsilon_w$, and $\epsilon_{zz}^{-1}=(1-f)/\varepsilon_b+f/\varepsilon_w$, $f=L_{QW}/L_{MQW}$. We assume for simplicity that the QWs have rectangular shapes.

APPENDIX B: RESONANT CONTRIBUTION FROM POLARITON MODE

Discussing the relationship between reflectivity (absorptivity) minima (maxima) and the eigenfrequences of the eigenmodes in the TIR geometry it is convenient to rewrite Eq. (10) into the form

$$r=(1-u)/(1+u)=(2-\mathcal{L})/\mathcal{L} \tag{B1}$$

with $\mathcal{L}=1+u$ and

$$u=\frac{1-r_{01}}{1+r_{01}}\frac{\mathcal{T}_{11}-\mathcal{T}_{21}}{\mathcal{T}_{11}+\mathcal{T}_{21}}, \tag{B2}$$

where $\mathcal{T}_{ij}\equiv[\mathbf{T}_{1,m+1}]_{ij}$. The matrix $\mathbf{T}_{1,m+1}$ is defined by relation $\mathbf{T}=\mathbf{I}_{0,1}\mathbf{T}_{1,m+1}$. (We assume that $\mathcal{T}_{11}+\mathcal{T}_{21}\neq 0$.)

Substituting Eq. (B1) into Eq. (11) we get

$$A=u'/|1+u|^2=4(\mathcal{L}'-1)/|\mathcal{L}|^2. \tag{B3}$$

It is obvious that the above expression has a physical meaning only for the real frequency ω.

The virtual mode Eq. (12) can be rewritten as

$$\mathcal{L}=1+u=0. \tag{B4}$$

Since we consider the radiative modes, the quantities $\mathcal{L}$ and u appearing in the above equation should be treated as functions of the complex frequency $\tilde{\omega}=\omega'+i\omega''$ even in the absence of the losses. The losses can be included assuming that $\mathcal{L}$ and u are also functions of the phenomenological damping parameters $\bar{\gamma}=(\bar{\gamma}_1,\bar{\gamma}_2,\bar{\gamma}_3,\ldots,\bar{\gamma}_q)$. These parameters describe the dissipation in all absorptive media of the considered structure. If $\tilde{\omega}$ is near the frequency of a well-separated virtual mode ν, then u can be approximated by the linear expansion[32] (the single-pole approximation)

$$u(\tilde{\omega},\bar{\boldsymbol{\gamma}}) = a_\nu + b_\nu\tilde{\omega} + \sum_{\alpha=1}^{q} c_{\nu,\alpha}\bar{\gamma}_\alpha, \tag{B5}$$

where the coefficients a_ν, b_ν, and $c_{\nu,\alpha}$ are, in general, complex quantities.

Let us assume for a moment that the dissipation is absent, i.e., $c_{\nu,\alpha}=0$. This implies the vanishing of the absorptance A. Consequently, we can take $u'(\tilde{\omega}=\omega,\bar{\boldsymbol{\gamma}}=0)=0$. Thus, parameters a_ν and b_ν can be treated as imaginary quantities. Taking this fact into account and remembering that $\tilde{\omega}_\nu$ denotes the (complex) mode frequency in the absence of dissipation, we get

$$a_\nu = -i\omega'_\nu/\omega''_\nu, \quad b_\nu = -i/\omega''_\nu. \tag{B6}$$

Employing Eqs. (B4)–(B6) we find, after some manipulations, that in the single-pole approximation the expression for the complex function $\mathcal{L}(\tilde{\omega}=\omega,\bar{\boldsymbol{\gamma}})$ reduces to the form

$$\mathcal{L}_\nu(\tilde{\omega}=\omega,\bar{\boldsymbol{\gamma}}) = \omega''_\nu/\omega''_\nu + i(\omega-\omega'_\nu)/\omega''_\nu = (i/\omega''_\nu)(\omega-\tilde{\omega}_\nu). \tag{B7}$$

Substituting the above relation it into Eq. (B3) we get Eq. (14).

APPENDIX C: TWO-OSCILLATOR MODEL

1. Dispersion relations and Hopfield coefficients

Let us assume that the behavior of the photonic mode c_n and the electronic mode $\mathcal{D}_n$ is well modeled by the two oscillators of frequencies $\omega_{c_n}(k_x)$ and ω_{IT} coupled by an energy $\Omega_R^{(n)}(\theta_n)\equiv\hat{V}_{nn}\sin\theta_n$. The coupling Hamiltonian is now a 2×2 matrix and the polariton dispersion relations are the solutions of the following matrix determinant:

$$\mathcal{M}_n(k_x,\omega) \equiv (\omega_{\mathrm{IT}}-\omega)[\omega_{c_n}(k_x)-\omega] - [\Omega_R^{(n)}(\theta_n)]^2 = 0. \tag{C1}$$

These solutions have a well-known form

$$\omega_{\pm n}(k_x) = \frac{\omega_{\mathrm{IT}}+\omega_{c_n}(k_x)}{2} \pm \frac{1}{2}\sqrt{\delta_n^2(k_x)+4[\Omega_R^{(n)}(\theta_n)]^2}, \tag{C2}$$

where $\delta_n(k_x)=\omega_{c_n}(k_x)-\omega_{\mathrm{IT}}$. From the above equation we find that the coupling between the electronic and photonic modes leads to the anticrossing of the upper $(+n\equiv U_n)$ and lower $(-n\equiv L_n)$ polariton branches. Rabi splitting frequency, i.e., the minimal separation between the above-mentioned branches, is given by $2\Omega_{R_{res}}^{(n)}=2\Omega_R^{(n)}(\theta_n^{res})$, where $\theta_n^{res}\equiv\theta_n(k_n^{res})$ and k_n^{res} is determined by relation $\omega_{c_n}(k_n^{res})=\omega_{\mathrm{IT}}$.

The $\pm n$th branch is a coherent mixture of the c_n and $\mathcal{D}_n$ states whose fractions are given by Hopfield coefficients $\mathcal{X}_{\pm n}(k_x)$ and $\mathcal{C}_{\pm n}(k_x)$. The electronic (photonic) weight is quantified by $\mathcal{X}_{\pm n}^2$ $(\mathcal{C}_{\pm n}^2)$. The expressions for these weights can be written as[27,40]

$$\mathcal{X}_{\pm n}^2(k_x) = \frac{\mp\delta_n(k_x)+\sqrt{\delta_n^2(k_x)+4[\Omega_R^{(n)}(\theta_n)]^2}}{2\sqrt{\delta_n^2(k_x)+4[\Omega_R^{(n)}(\theta_n)]^2}}, \tag{C3}$$

$$\mathcal{C}_{\pm n}^2(k_x) = 1-\mathcal{X}_{\pm n}^2(k_x). \tag{C4}$$

At $k_x=k_n^{res}$ the polaritons are half electronic and half photonic, that is, $\mathcal{X}_{\pm n}^2=\mathcal{C}_{\pm n}^2=1/2$. When $k_x\neq k_n^{res}$ it is convenient to write $\mathcal{X}_{\pm n}^2(k_x)$ in terms of the dimensionless parameter $F_n(k_x)=2\Omega_R^{(n)}(\theta_n)/\delta_n(k_x)$ as

$$\mathcal{X}_{\pm n}^2(k_x) = \frac{\mp1+\sqrt{1+F_n^2(k_x)}}{2\sqrt{1+F_n^2(k_x)}}. \tag{C5}$$

One can check that when $F_n^2(k_x)\ll1$ the following approximation is valid: $\mathcal{X}_{+n}^2(k_x)\approx\mathcal{C}_{-n}^2(k_x)\approx F_n^2(k_x)/4=[\Omega_R^{(n)}(\theta_n)]^2/\delta_n^2(k_x)$. Thus in the limit of large vectors $(F_n(k_x)\to0)$ the upper branch becomes photonic, that is, $\mathcal{X}_{+n}^2\approx0$ and $\mathcal{C}_{+n}^2\approx1$, and the lower branch becomes electronic, that is, $\mathcal{X}_{-n}^2\approx1$ and $\mathcal{C}_{-n}^2\approx0$.

Employing Eq. (13) we can eliminate k_x from Eq. (C1). Assuming for simplicity that the coupling strength between c_n and $\mathcal{D}_n$ modes is not too large (or more precisely, assuming that $\Omega_{R_{res}}^{(n)}/\cos\theta_n^{res}\ll\omega_{\mathrm{IT}}$ and φ is close to φ_n^{res}) we obtain the following expression for the polariton mode dispersion in the φ-ω plane:

$$\omega_{\pm n}(\varphi) = \frac{\omega_{\mathrm{IT}}+\omega_{c_n}(\varphi)}{2} \pm \frac{1}{2}\sqrt{\bar{\delta}_n^2(\varphi)+4[\bar{\Omega}_R^{(n)}(\varphi)]^2}, \tag{C6}$$

where $\omega_{c_n}(\varphi)=n\omega_\perp/\cos(\varphi)=n\omega_{c_1}(\varphi)$, $\bar{\delta}_n(\varphi)=\omega_{c_n}(\varphi)-\omega_{\mathrm{IT}}$, and $\bar{\Omega}_R^{(n)}(\varphi)=\hat{V}_{nn}\tan\varphi$.

As it has been mentioned (see also Fig. 4) polariton energies $\omega_{-1}(\varphi)$ and $\omega_{+1}(\varphi)$ corresponding to the same angle $\varphi=\varphi_1^{res}$ correspond to the different values of k_x given by

$$\bar{k}_{\pm1}^{res} = \omega_{\pm1}(\varphi_1^{res})\sin(\varphi_1^{res})\varepsilon_s^{1/2}/c.$$

Equivalently we can also use the following relation:

$$\omega_{\mathrm{IT}} \pm \bar{\Omega}_{R_{res}} = \omega_{\pm1}(\bar{k}_{\pm1}^{res}). \tag{C7}$$

To simplify further discussion we employ the fact that when $k_{z,1}^2\ll(k_1^{res})^2$ and $\Omega_{R_{res}}\ll\omega_{\mathrm{IT}}$, like in the systems considered here, then, to a good approximation, $\theta_1(\bar{k}_{\pm1}^{res})$ can be replaced by $\theta_1(k_1^{res})$. Moreover, we can neglect the difference between $|\delta_1(\bar{k}_{+1}^{res})|$ and $|\delta_1(\bar{k}_{-1}^{res})|$ taking $|\delta_1(\bar{k}_{+1}^{res})|=|\delta_1(\bar{k}_{-1}^{res})|\equiv\delta_1^{res}$. Thus the parameter $F_1(\bar{k}_{\pm1}^{res})$, appearing in the expression for the Hopfied coefficients [Eq. (C5)], can be approximated as $F_1(\bar{k}_{\pm1}^{res})\approx2\Omega_{R_{res}}/\delta_1^{res}$. Using these simplifications and Eq. (C7) we get useful relation given by Eq. (32).

We should remember that in a real cavity, the electronic and photonic modes are coupled to a continuum of modes. It leads to the dissipation. This can be accounted for by introducing, in the coupling Hamiltonian [or equivalently in the matrix determinant Eq. (C1)], complex frequencies $\tilde{\omega}_{\mathrm{IT}}=\omega_{\mathrm{IT}}-i\gamma_{\mathrm{IT}}$ and $\tilde{\omega}_{c_n}(k_x)=\omega_{c_n}(k_x)-i\hat{\gamma}_{c_n}(k_x)$, where $\hat{\gamma}_{c_n}(k_x)$ is the decay rate of the c_n cavity mode. The matrix determinant [Eq. (C1)] takes now the form

$$\tilde{\mathcal{M}}_n(k_x,\omega) \equiv [\tilde{\omega}_{c_n}(k_x) - \omega](\tilde{\omega}_{\mathrm{IT}} - \omega) - [\Omega_R^{(n)}(\theta_n)]^2. \tag{C8}$$

The polariton frequencies resulting from this determinant are complex numbers. For $k_x = k_n^{res}$ one obtains

$$\tilde{\omega}_{\pm n}(k_n^{res}) = \omega_{\mathrm{IT}} - i\frac{\gamma_{\mathrm{IT}} + \hat{\gamma}_{c_n}^*}{2} \pm \frac{1}{2}\sqrt{4(\Omega_{R_{res}}^{(n)})^2 - (\gamma_{\mathrm{IT}} - \hat{\gamma}_{c_n}^*)^2}, \tag{C9}$$

where $\hat{\gamma}_{c_n}^* = \hat{\gamma}_{c_n}(k_n^{res})$. It can be observed that the polariton frequency depends crucially on the sign of the expression below the square root. If $(2\Omega_{R_{res}}^{(n)})^2 \gg (\gamma_{\mathrm{IT}} - \hat{\gamma}_{c_n}^*)^2$, then $\omega_{\pm n}(k_n^{res})$ exhibit the frequency splitting already encountered: it is the SCR. If the above-mentioned inequality is not fulfilled, the mode splitting disappears and the system is in the weak-coupling regime.

As it has been mentioned, for the interpretation of the angle-resolved absorption spectra the polariton dispersion relation in the φ-ω plane is required. Employing Eq. (13) and restricting to the SCR we can rewrite [for ω not to far from $\omega_{c_n}(\varphi)$] the matrix determinant [Eq. (C8)] into the following form:

$$\overline{\tilde{\mathcal{M}}}_n(\varphi,\omega) \approx [\tilde{\omega}_{c_n}(\varphi) - \omega](\tilde{\omega}_{\mathrm{IT}} - \omega) - [\bar{\Omega}_R^{(n)}(\varphi)]^2, \tag{C10}$$

where $\tilde{\omega}_{c_n}(\varphi) = \omega_{c_n}(\varphi) - i\gamma_{c_n}(\varphi)$. The quantity $\gamma_{c_n}(\varphi) = \hat{\gamma}_{c_n}(k_x = k_{z,n}\tan\varphi)/\cos^2\varphi$ is the decay rate of the c_n cavity mode radiating at the angle φ. Note that, in general, the cavity mode decay rate contains the radiative $\gamma_{c_n}^{rad}$ and the absorptive $\gamma_{c_n}^{abs} = \gamma_{c_n} - \gamma_{c_n}^{rad}$ contributions. $\gamma_{c_n}^{rad}$ is connected with finite transmitivity (T_c) of the coupling mirror. The absorptive contribution $\gamma_{c_n}^{abs}$ appears due to the absorptive losses in the passive MC (see Appendix D).

Solving the equation

$$\overline{\tilde{\mathcal{M}}}_n(\varphi,\omega) = 0, \tag{C11}$$

we get the expression for the angular dependence of the complex mode frequencies $\tilde{\omega}_{\pm n}(\varphi)$ given by Eq. (23). It is convenient to separate the real and imaginary parts of $\tilde{\omega}_{\pm n}(\varphi)$. They can be written as

$$\omega'_{\pm n}(\varphi) = \frac{\omega_{\mathrm{IT}} + \omega_{c_n}(\varphi)}{2} \pm \frac{(a_n^2 + b_n^2)^{1/4}}{2}\cos\left(\frac{\phi_n}{2}\right), \tag{C12}$$

$$-\omega''_{\pm n}(\varphi) = \frac{\gamma_{\mathrm{IT}} + \gamma_{c_n}(\varphi)}{2} \mp \frac{(a_n^2 + b_n^2)^{1/4}}{2}\sin\left(\frac{\phi_n}{2}\right), \tag{C13}$$

where

$$a_n \equiv a_n(\varphi) = \bar{\delta}_n^2(\varphi) - [\gamma_{c_n}(\varphi) - \gamma_{\mathrm{IT}}]^2 + [2\bar{\Omega}_R^{(n)}]^2,$$

$$b_n \equiv b_n(\varphi) = -2\bar{\delta}_n(\varphi)[\gamma_{c_n}(\varphi) - \gamma_{\mathrm{IT}}],$$

$$\tan\phi_n = b_n/a_n \quad (0 < \phi_n \le \pi).$$

The SCR is achieved when $|b_n/a_n| \ll 1$. In this regime the influence of the dissipation on $\omega'_{\pm n}(\varphi)$ can be neglected in the first approximation. In other words, the φ dependence of $\omega'_{\pm n}$ can be approximated by Eq. (C6).

Performing appropriate expansion in Eq. (C13) one can check that the polariton relaxation rate $\gamma_{\pm n}(\varphi) \equiv -\omega''_{\pm n}(\varphi)$ can be written in the terms of $\gamma_{c_n}(\varphi)$ and γ_{IT} as

$$\gamma_{\pm n}(\varphi) = \bar{\mathcal{C}}_{\pm n}^2(\varphi)\gamma_{c_n}(\varphi) + \bar{\mathcal{X}}_{\pm n}^2(\varphi)\gamma_{\mathrm{IT}}, \tag{C14}$$

where the modified Hopfield coefficients $\bar{\mathcal{C}}_{\pm n}$ and $\bar{\mathcal{X}}_{\pm n}$ are given by Eqs. (C3) and (C4) with $\delta_n(k_x)$ replaced by $\bar{\delta}_n(\varphi)$ and $\Omega_R^{(n)}(\theta_n)$ replaced by $\bar{\Omega}_R^{(n)}(\varphi)$. [In the case of Eq. (C5) $F_n(k_x)$ should be replaced by $\overline{F}_n(\varphi) = 2\bar{\Omega}_R^{(n)}(\varphi)/\bar{\delta}_n(\varphi)$.] It implies that at resonance, $\varphi = \varphi_n^{res}$, the decay rate of the upper and lower polariton branches are the same and equal to $\gamma_{\pm n} = \gamma_n^* \equiv (\gamma_{c_n}^* + \gamma_{\mathrm{IT}})/2$, where $\gamma_{c_n}^* \equiv \gamma_{c_n}(\varphi_n^{res})$.

2. Absorption spectra

It is instructive to use the two-oscillator model to further explore the optical properties of the MC as a function of different parameters. The application of the input-output formalism makes it possible to calculate the absorption of the MC connected with the nth polariton branches (for details see Ref. 27). Employing an approach analogous to that developed in the above-mentioned paper we find that k_x-resolved absorption spectrum (connected with the nth order polariton branches) can be written in the form

$$A_n(\omega) = \frac{4\hat{\gamma}_{c_n}(k_x)\gamma_{\mathrm{IT}}[\Omega_R^{(n)}(\theta_n)]^2}{|\tilde{\mathcal{M}}_n(k_x,\omega)|^2}. \tag{C15}$$

In obtaining this equation we have assumed, following Giacobino *et al.*,[27] that $\hat{\gamma}_{c_n}^{abs} = 0$. One can check that including the absorptive contribution in the equation of motion of the photonic oscillators induces the following substitution in the numerator of Eq. (C15):

$$\gamma_{\mathrm{IT}}[\Omega_R^{(n)}(\theta_n)]^2 \to \gamma_{\mathrm{IT}}[\Omega_R^{(n)}(\theta_n)]^2 + \hat{\gamma}_{c_n}^{abs}[(\omega - \omega_{\mathrm{IT}})^2 + \gamma_{\mathrm{IT}}^2]. \tag{C16}$$

However, we should remember that in experiments not k_x but φ is fixed. Performing appropriate manipulations one can obtain from Eqs. (13), (C8), (C15), and (C16) an expression for the angle-resolved absorption spectrum described by Eq. (25).

APPENDIX D: MULTIBEAM INTERFERENCE APPROACH

Let us assume, like in Sec. II B, that the MQW (with period L_{MQW} and number of the wells N_{QW}) is located between the coupling mirror (at $z=0$) and the totally reflecting back mirror (at $z=L_{\mathrm{MC}}$). The coupling and back mirrors are characterized by the amplitude reflection (transmission) coefficients r_c (t_c) and r_b (t_b), respectively. The difference be-

tween the dielectric constant of the substrate material (ε_s), the barrier material (ε_b), and the well material (ε_w) is assumed to be vanishingly small.

For realistic values of the QW parameters the quantity Λ_{QW} [see Eq. (A4)] is very small. Thus, the expressions for the reflection and transmission coefficients of the sheet [modeling Q2DEG in QWs] can be approximated by

$$r^{2\mathrm{D}} \cong 0, \quad t^{2\mathrm{D}} \cong e^{-\Lambda_{\mathrm{QW}}/2}. \tag{D1}$$

Omitting the light reflection by the Q2DEG is consistent with a traveling-wave approximation discussed in our previous paper.[22] In this limit we can calculate the reflectance and absorptance of the above-mentioned MQW-MC system employing a standard multibeam interference analysis (see, e.g., Refs. 17 and 41). In this approach the complex amplitude of the wave reflected by the system, A_r, is treated as a sum of the partially reflected components A_{r1}, A_{r2}, A_{r3},.... Taking into account Eq. (D1) we get the expression for the reflectivity of the system $r^{\mathrm{MB}}=A_r/A_i$ (A_i is the amplitude of the incident light) as

$$\begin{aligned} r^{\mathrm{MB}} &= r_c + t_c t_c r_b e^{i2\Phi_{\mathrm{tot}}-\mathcal{A}}[1 + r_c r_b e^{i2\Phi_{\mathrm{tot}}-\mathcal{A}} \\ &\quad + (r_c r_b e^{i2\Phi_{\mathrm{tot}}-\mathcal{A}_{\mathrm{tot}}})^2 + \cdots] \\ &= \frac{r_c + (t_c^2 - r_c^2) r_b e^{i2\Phi_{\mathrm{tot}}-\mathcal{A}}}{1 - r_c r_b e^{i2\Phi_{\mathrm{tot}}-\mathcal{A}}}. \end{aligned} \tag{D2}$$

We have defined (i) the half round-trip (total) phase change $\Phi_{\mathrm{tot}}=\Phi_{\mathrm{MC}}+\Phi_{\mathrm{MQW}}$, where $\Phi_{\mathrm{MC}}=\cos\varphi K\sqrt{\varepsilon_w}L_{\mathrm{MC}}$ and $\Phi_{\mathrm{MQW}}=N_{\mathrm{QW}}\,\mathrm{Im}\,\Lambda_{\mathrm{QW}}/2$ and (ii) the half round-trip (total) absorptance $1-e^{-\mathcal{A}_{\mathrm{tot}}}$, where $\mathcal{A}=\mathcal{A}_{\mathrm{MQW}}+\mathcal{A}_{\mathrm{MC}}$ and $\mathcal{A}_{\mathrm{MQW}}=N_{\mathrm{QW}}\,\mathrm{Re}\,\Lambda_{\mathrm{QW}}$. $\mathcal{A}_{\mathrm{MC}}$ determines the single pass absorptance of the passive MC.

In further discussion we utilize the following relations: $r_b=-\sqrt{R_b}$, $r_c=-\sqrt{R_c}$, $t_c=i\sqrt{T_c}$, and $T_c=1-R_c$, valid for dielectric mirrors.[42] In the presence of the losses in the mirrors the following relations are valid $R_b=1-A_b$ and $R_c=1-T_c-A_c$, where A_b (A_c) denotes the absorptance of the bottom (coupled) mirror). To get simple analytical results we restrict ourselves to the case when T_c and $\mathcal{A}_{\mathrm{tot}}[=\mathcal{A}+(A_c+A_b)/2]$ can be treated as small quantities. Employing the above-mentioned simplifying assumptions we can reduce Eq. (D2) to the form

$$r^{\mathrm{MB}} = \frac{-1 + \frac{T_c + A_c}{2} + \left(1 - \frac{A_c}{2} - \mathcal{A}_{\mathrm{tot}}\right)\exp(i2\Phi_{\mathrm{tot}})}{1 - \left(1 - \frac{T_c}{2} - \mathcal{A}_{\mathrm{tot}}\right)\exp(i2\Phi_{\mathrm{tot}})}. \tag{D3}$$

The dispersion equation for the polariton modes, resulting from Eq. (D3) can be written as

$$\left(1 - \frac{T_c}{2} - \mathcal{A}_{\mathrm{tot}}\right)\exp(i2\Phi_{\mathrm{tot}}) = 1. \tag{D4}$$

Neglecting the intersubband transitions ($\mathcal{A}_{\mathrm{MQW}}=\Phi_{\mathrm{MQW}}=0$) we get from Eq. (D4) the following expressions for the radiative and absorptive components of the cavity decay rates:

$$\gamma_{c_n}^{rad}(\varphi) = T_c\omega_{c_1}(\varphi)/4\pi, \tag{D5}$$

$$\gamma_{c_n}^{abs}(\varphi) = (2\mathcal{A}_{\mathrm{MC}} + A_c + A_b)\omega_{c_1}(\varphi)/4\pi. \tag{D6}$$

[The expression for $\gamma_{c_n}^{rad}(\varphi)$ presented in Ref. 6 contains misprint.]

To proceed further we define the quantity $\Phi_{\mathrm{tot}}^{(n)}=\Phi_{\mathrm{MQW}}-\Phi_{\mathrm{MC}}^{(n)}$, where $\Phi_{\mathrm{MC}}^{(n)}=\pi n-\Phi_{\mathrm{MC}}=\pi[\omega_{c_n}(\varphi)-\omega]/\omega_{c_1}(\varphi)$. Then we restrict ourselves to a frequency range where this quantity is very small.[17,42] In this limit the exponential term appearing in Eqs. (D3) and (D4) can be expanded in the power series and the dispersion Eq. (D4) reduces to

$$T_c + 2\mathcal{A}_{\mathrm{tot}} - i4\Phi_{\mathrm{tot}}^{(n)} = 0. \tag{D7}$$

The expression for the absorptance of the MQW-MC system $A^{\mathrm{MB}}=1-|r^{\mathrm{MB}}|^2$ simplifies to

$$A_n^{\mathrm{MB}} = \frac{8\mathcal{A}_{\mathrm{tot}}T_c}{(T_c + 2\mathcal{A}_{\mathrm{tot}})^2 + (4\Phi_{\mathrm{tot}}^{(n)})^2}. \tag{D8}$$

One can check that the RWA Eq. (D7) [Eq. (D8)] reduces to Eq. (C11) [Eq. (24)].

As it has been mentioned in Sec. I, the results reported in Ref. 14 have been interpreted employing a simplified semiclassical approach developed by Zhu *et al.*[17] Referring to this paper, the authors of Ref. 14 assume that in the SCR the resonances of the MQW-MC system (and consequently the absorption peaks) should occur for the (real) frequencies at which the total round-trip phase shifts are multiple of 2π. The above condition can be written in the equivalent form as $\Phi_{\mathrm{tot}}^{(n)}(\omega)=0$. It leads (in the RWA) to the following implicit expression for the frequencies of the nth order polariton branches at $\varphi=\varphi_1^{res}$:

$$\frac{n\omega_{\mathrm{IT}} - \omega}{\omega_{\mathrm{IT}} - \omega} = \frac{\bar{\Omega}_{R_{res}}^2}{\gamma_{\mathrm{IT}}^2 + (\omega_{\mathrm{IT}} - \omega)^2}. \tag{D9}$$

Since in the SCR the inequality $\bar{\Omega}_{R_{res}}^2 \gg \gamma_{\mathrm{IT}}^2$ is fulfilled, for $n=1$ this formula gives a well-known expression $\omega_{\mathrm{IT}} \pm \bar{\Omega}_{R_{res}}$ for the location of the two main absorption peaks. Unfortunately, the above formula does not work correctly when $n>1$. For example, taking a realistic value of $\gamma_{\mathrm{IT}}=0.03\ \omega_{\mathrm{IT}}$ one finds, in agreement with estimations reported by Dupont *et al.*[14] (see Fig. 5 in the above paper), that for $n=2$ Eq. (D9) has no solutions as long as $\bar{\Omega}_{R_{res}} \lesssim 0.25\ \omega_{\mathrm{IT}}$. One can check that this is entirely due to the presence of the "dissipation" terms (the first two terms) in Eq. (D7). These terms are neglected in the approach leading to Eq. (D9). It has a good justification in the case of the U_1 and L_1 branches. However, when the eigenmode frequency is close to ω_{IT} (like in the case of the $L_{n>1}$ branches), the term $\mathcal{A}_{\mathrm{tot}}$ (more precisely $\mathcal{A}_{\mathrm{MQW}}$) cannot be treared as a very small and consequently the above-mentioned approximation breaks down. Fortunately, the problem can be overcome when we completely neglect the dissipation in Eq. (D9). In the limit $\gamma_{\mathrm{IT}}=0$ (and $\varphi=\varphi_1^{res}$) Eq. (D9) becomes equivalent to Eq. (C6).

[1] D. Dini, R. Kohler, A. Tredicucci, G. Biasiol, and L. Sorba, Phys. Rev. Lett. **90**, 116401 (2003).
[2] E. Dupont, H. C. Liu, A. J. SpringThorpe, W. Lai, and M. Extavour, Phys. Rev. B **68**, 245320 (2003).
[3] D. A. Dahl and L. J. Sham, Phys. Rev. B **16**, 651 (1977).
[4] A. Liu, Phys. Rev. B **55**, 7101 (1997).
[5] A. A. Anappara, S. De Liberato, A. Tredicucci, C. Ciuti, G. Biasiol, L. Sorba, and F. Beltram, Phys. Rev. B **79**, 201303(R) (2009).
[6] M. Załużny and W. Zietkowski, Phys. Rev. B **78**, 033305 (2008).
[7] A. A. Anappara, A. Tredicucci, G. Biasiol, and L. Sorba, Appl. Phys. Lett. **87**, 051105 (2005).
[8] A. A. Anappara, A. Tredicucci, G. Biasiol, and L. Sorba, Appl. Phys. Lett. **89**, 171109 (2006).
[9] L. Sapienza, A. Vasanelli, R. Colombelli, C. Ciuti, Y. Chassagneux, C. Manquest, U. Gennser, and C. Sirtori, Phys. Rev. Lett. **100**, 136806 (2008).
[10] Y. Todorov, P. Jouy, A. Vasanelli, L. Sapienza, R. Colombelli, U. Gennser, and C. Sirtori, Appl. Phys. Lett. **93**, 171105 (2008).
[11] S. De Liberato and C. Ciuti, Phys. Rev. B **79**, 075317 (2009).
[12] G. Günter, A. A. Anappara, J. Hees, A. Sell, A. Biasiol, L. Sorba, S. De Liberato, C. Ciuti, A. Tredicucci, A. Leitenstorfer, and R. Huber, Nature (London) **458**, 178 (2009), and references therein.
[13] J. Plumridge, E. Clark, R. Murray, and C. Philips, Solid State Commun. **146**, 406 (2008).
[14] E. Dupont, J. A. Gupta, and H. C. Liu, Phys. Rev. B **75**, 205325 (2007).
[15] Y. Todorov, A. M. Andrews, I. Sagnes, R. Colombelli, P. Klang, G. Strasser, and C. Sirtori, Phys. Rev. Lett. **102**, 186402 (2009).
[16] R. Colombelli, C. Ciuti, Y. Chassangneux, and C. Sirtori, Semicond. Sci. Technol. **20**, 985 (2005).
[17] Y. Zhu, D. J. Gauthier, S. E. Morin, Q. Wu, H. J. Carmichael, and T. W. Mossberg, Phys. Rev. Lett. **64**, 2499 (1990).
[18] E. L. Ivchenko, M. A. Kaliteevski, A. V. Kavokin, and A. I. Nesvizhskii, J. Opt. Soc. Am. B **13**, 1061 (1996).
[19] M. Richard, R. Romestain, R. Andre, and L. S. Dang, Appl. Phys. Lett. **86**, 071916 (2005).
[20] A. I. Tartakovskii, V. D. Kulakovskii, Yu. I. Koval, T. B. Borzenko, A. Forchel, and J. P. Reithmaier, Zh. Eksp. Teor. Fiz. **87**, 723 (1998); A. I. Tartakovskii, V. D. Kulakovskii, A. Forchel, and J. P. Reithmaier, Phys. Rev. B **57**, R6807 (1998).
[21] H. Kondo, Y. Yamamoto, A. Takeda, S. Yamamoto, and H. Kurisu, J. Lumin. **128**, 777 (2008).
[22] M. Załużny and C. Nalewajko, Phys. Rev. B **59**, 13043 (1999).
[23] G. Panzarini and L. C. Andreani, Phys. Rev. B **52**, 10780 (1995).
[24] J. Wainstain, C. Delalande, D. Gendt, M. Voos, J. Bloch, V. Thierry-Mieg, and R. Planel, Phys. Rev. B **58**, 7269 (1998).
[25] S. Pau, G. Björk, H. Cao, E. Hanamura, and Y. Yamamoto, Solid State Commun. **98**, 781 (1996).
[26] R. Houdre, R. P. Stanley, and M. Ilegems, Phys. Rev. A **53**, 2711 (1996).
[27] E. Giacobino, J.-P. Karr, G. Messin, H. Eleuch, and A. Bass, C. R. Phys. **3**, 41 (2002).
[28] E. M. Goldys, G. C. La Rocca, and F. Bassani, Phys. Rev. B **61**, 10346 (2000); P. Michetti and G. C. La Rocca, *ibid.* **71**, 115320 (2005).
[29] M. V. Erementchouk, L. I. Deych, and A. A. Lisyansky, Phys. Rev. B **71**, 235335 (2005).
[30] T. Shih, K. Reimann, M. Woerner, T. Elsaesser, I. Waldmüller, A. Knorr, R. Hey, and K. H. Ploog, Phys. Rev. B **72**, 195338 (2005).
[31] R. D. King-Smith and J. C. Inkson, Phys. Rev. B **36**, 4796 (1987).
[32] K. L. Kliewer and R. Fuchs, Phys. Rev. **144**, 495 (1966).
[33] M. Załużny and W. Ziętkowski, Solid State Commun. **125**, 287 (2003).
[34] M. F. Pereira, Jr., Phys. Rev. B **75**, 195301 (2007).
[35] A. V. Kavokin, Phys. Rev. B **57**, 3757 (1998).
[36] A. Vasanelli (private communication).
[37] T. Ando, A. Fowler, and F. Stern, Rev. Mod. Phys. **54**, 437 (1982).
[38] M. Załużny and W. Zietkowski, Physica E **13**, 370 (2002).
[39] M. Załużny and C. Nalewajko, Phys. Rev. B **68**, 233305 (2003).
[40] B. Sermage, S. Long, I. Abram, J. Y. Marzin, J. Bloch, R. Planel, and V. Thierry-Mieg, Phys. Rev. B **53**, 16516 (1996).
[41] J. Liao, X. J. Zhang, F. Xu, X. Z. Fan, H. T. Wang, and N. B. Ming, Appl. Phys. B: Lasers Opt. **75**, 865 (2002).
[42] G. P. Agrawal and H. J. Carmichael, Phys. Rev. A **19**, 2074 (1979).